Experimental study on rise velocities of single bubbles in liquid metal under the influence of strong horizontal magnetic fields in a flat vessel

Strumpf, E.;

Originally published:

September 2017

International Journal of Multiphase Flow 97C(2017), 168-185

DOI: https://doi.org/10.1016/j.ijmultiphaseflow.2017.08.001

Perma-Link to Publication Repository of HZDR:

https://www.hzdr.de/publications/Publ-24634

Experimental study on rise velocities of single bubbles in liquid metal under the influence of strong horizontal magnetic fields in a flat vessel

Erik Strumpf

Helmholtz-Zentrum Dresden-Rossendorf (HZDR), MHD Department, PO Box 510199, 01314 Dresden, Germany

Abstract. The ascent of single argon bubbles with equivalent diameters (d_{eq}) between 3.43 and 6.28 mm is investigated at room temperature in a flat, cubic vessel by means of Ultrasound Doppler Velocimetry (UDV). GaInSn is used as a working liquid and magnetic flux intensities up to $B \approx 0.918$ T are applied. A decelerating effect on the rise velocity is observed at lower, an accelerating effect at medium and a reduction at higher field strengths. Maximum velocities are achieved when $N/C_D \approx 1$, bubble paths are substantially rectilinear at $N/C_D > 2$. The mean ascent velocities are compared with literature and data of this work as well of other publications is provided in tables.

Keywords: bubble, rise velocity, liquid metal, magnetic field, ultrasound

1 Introduction

Apart from investigations of the pure hydrodynamic phenomenon of bubble ascent, the influence of a magnetic field on the behavior of gas bubbles in magnetic conducting liquids came into focus of different research groups within the last years. In 1977 Mori et al. [1] (further referred to as "Mori") provided quantitative data on the ascent of nitrogen bubbles in mercury under the influence of a horizontal uniform, static magnetic field (HMF) with magnetic flux densities up to B = 1.5 T. According to their conclusions the influence of a magnetic field is twofold. At lower magnetic flux densities the bubble rise velocity (of small bubbles) is increased, compared to the pure hydrodynamic case, whereas at higher field strengths a dampening effect was observed. Moreover, their data indicate that large bubbles ($Eo > 4$) are only decelerated with increasing field strength. In their paper in 2005 as well as in his PhD thesis in 2009 Zhang et al. [2], [3] ("C. Zhang") provided experimental data of argon bubbles in GaInSn under the influence of vertical magnetic fields (VMF) and HMF. They observed a quite ambivalent behavior depending on equivalent bubble diameter and magnetic field configuration. Their experimental setup was limited to a magnetic flux density of about 0.3 T ($N \approx 1$), which is not enough to observe phenomena in the regions where magnetic forces are predominant over viscosity and inertia. Several numerical calculations were conducted within the last years. Recently, Jin et al. [4] presented a literature overview on both experimental and numerical studies. A more complete overview is given in Table 1 where the basic structure of their summary is maintained. It is obvious that the focus of investigations on this topic is of computational nature, counting 17

Abbrevations

AMF	azimuthal magnetic field
C	computational
E	experimental
HMF	horizontal magnetic field
L,W,H	length, width, height
MF	magnetic fluid
N/A	not available
SD	standard deviation
UDV	ultrasound Doppler velocimetry
VMF	vertical magnetic field

Physical quantities

c	speed of sound
d_{eq}	sphere equivalent bubble diameter
f	bubble detachment frequency
g	gravitational acceleration
$\dot{m}$	gas mass flow rate
u	bubble ascent velocity
t	time
B	magnetic flux density
D_a	Inner diameter
D_i	Inner diameter
H_0	magnetic intensity
T	temperature
T_B	boiling temperature
T_M	melting temperature
η	dynamic viscosity
ρ	physical density
σ	static surface tension
σ_{el}	electrical conductivity
χ	aspect ratio

Dimensionless numbers

C_D	Drag coefficient	$C_D = 4\Delta\rho g d / 3\rho u^2$
Eo	Eötvös number	$Eo = \Delta\rho g d^2 / \sigma$
Ga	Galilei number	$Ga = g d^3 \rho^2 / \eta^2$
Ha	Hartmann number	$Ha = Bd(\sigma_{el}/\eta)^{-0.5}$
N	Stuart number	$N = \sigma_{el} B^2 d / \rho u$
Re	Reynolds number	$Re = \rho u d / \eta$
We	Weber number	$We = \rho u^2 d / \sigma$

publications on numerical simulation and 7 on experimental studies (not taking into account unpublished articles). In general, the validation of these numerical codes is done by comparison with the few available experimental results, most of all the data provided by Mori and C. Zhang. Consequently there is a need for comprehensive, experimental studies on this topic.
A quantitative study on the ascent velocity of argon bubbles in liquid GaInSn under the influence of static magnetic fields for different bubble sizes is presented and compared with literature. Measurement steps of magnetic flux density are chosen to be sufficiently small to provide detailed insight into bubble behavior at smaller and larger field strengths.
The paper is structured as follows: In chapter 2 the experimental setup as well as the data processing will be depicted, followed by experimental results and comparisons to simulations as well as other experiments (chapter 3), closing with conclusion and discussion in chapter 4. Data of this work as well as that of other authors (recalculated from the corresponding papers) is given in the appendix.

Table 1. Literature overview on the topic of ascending single bubbles under the influence of magnetic fields**.** Note that several authors don't provide detailed information on magnetic field strengths, bubble sizes or the gas - liquid configuration. Here those entries are labeled with N/A but more information can be found in the corresponding papers. (E - experimental, C - computational)

Year	Author	E/C	Gas & liquid	Field direction	Field strength	Bubble size
1977	Mori et al. [1]	E	N_2 & Hg	HMF	$B \approx 0$ - 1.5 T	$Eo \approx 0.88$ - 9.95
1995	Ueno et al. [5]	C	N/A	VMF	N/A	N/A
1995	Ishimoto et al. [6]	E	Vapour & hexane - based MF Air & kerosene – based MF	HMF HMF & VMF	$H_0 = 0$ - 115.3 kA/m $H_0 = 0$ - 18 kA/m	$d_{eq} \approx 0.8$ mm $d_{eq} \approx 2.3$ - 17.2 mm
1999	Ueno et al. [7]	C	N/A	VMF	$\Pi = \mu_0 H_0^2/\rho_L u_0^2 = 0$ - 15	N/A
1999	Nakatsuka et al. [8]	E	Air & N/A	HMF	$B \approx 0$ - 0.2 T	$d_{eq} \approx 1.5$ - 4.0 mm
2005	C. Zhang et al. [2]	E	Ar & GaInSn	VMF	$B \approx 0$ - 0.30 T	$Eo = 2.2$ - 6.6
2006	Tagawa [9]	C	Air & H_2O	AMF	$B = 1.7$ T	$Ga \approx 1000$
2008	Huang et al. [10]	E, C	Air & MF	VMF	$H_0 = 2200$ & 4900 A/m	$d_{eq} = 7.0$ mm
2008	Merrouche et al. [11]	C	N/A & GaInSn	VMF	$B = 0 \ldots 0.15$ T	$Eo = 3.4$
2008	Korlie et al. [12]	C	N/A	VMF	N/A	$Eo \approx 2.19$
2009	C. Zhang [3]	E	Ar & GaInSn	VMF HMF	$B \approx 0$ - 0.30 T	$Eo = 2.2$ - 6.6 $Eo = 2.7$ - 6.9
2010	Gaudlitz & Adams [13]	C	Air & Water with σ_{el} of Hg	VMF	$B = 0.16$ T	N/A
2010	Shibasaki et al. [14]	C	N/A	VMF	$Ha = 0, 30, 50, 100, 150$	$d_{eq} = 10.0$ mm
2010	Kumazawa et al. [15][a]	E	Ar & H_2O + NaCl	HMF	$B = 0$ - 7 T	$d_{eq} = 3.0$ mm
2012	Pan & Ni [16]	C	N/A	HMF	$Ha = 0$ & 50	N/A
2012	Ansari et al. [17]	C	N/A	VMF	$B = 0$ - 0.07 T	$Eo = 36$
2014	J. Zhang & Ni [18]	C	N_2 & Hg Ar & GaInSn	VMF	$B = 0$ - 1.5 T $B = 0$ - 0.3 T	$d_{eq} = 5.6$ mm $Eo = 1.2$ - 2.5
2014	Schwarz et al. [19]	C	Ar & GaInSn	VMF	$B = 0$ - 2.0 T	$Eo = 2.5$
2014	J. Zhang & Ni [20]	C	Ar & GaInSn	VMF	$B = 0$ - 0.5 T	$Eo = 0.74$ - 4.9
2016	J. Zhang et al. [21]	C	Ar & GaInSn	HMF	$B = 0$ - 4 T	$Eo = 2.2$ & 4.9
2016	Tian et al. [22]	C	N/A	VMF	$B = 0$ - 0.4 T	$d_{eq} = 4.0$ - 12.0 mm
2016	Jin et al. [4]	C	Ar & Steel	HMF	$B = 0$ - 0.54 T	$Eo = 0.51, 1.43, 2.80$
2016	Yamasaki & Yamaguchi [23]	C	Air & N/A	VMF	$B = 0$ - 0.218 T	$Eo = 38.2$
2016	Wang et al. [24][b]	E	Ar & GaInSn	HMF	$B \approx 0$ - 2.0 T	$Eo \approx 1.12$ - 3.67
2016	Richter et al. [25]	E	Ar & GaInSn	HMF	$B \approx 0$ - 0.505 T	$d_{eq} \approx 4.6$ & 6.1 mm
2016	Present study	E	Ar & GaInSn	HMF	$B \approx 0$ - 0.919 T	$d_{eq} \approx 3.2$ - 6.28 mm

[a]: Conference paper of Iwai & Furuhashi (2008) [26] not listed here because it is basically the same study
[b]: Paper is submitted. Author has insight to the basic results due to a conference talk of Wang at the MTLM 2015, Dresden.

2 Experimental setup and data processing

A narrow, cubic vessel (Fig. 1), made of acrylic glass is used to investigate the ascent of single bubbles in GaInSn. It is filled up to a height of 144 mm which results in an aspect ratio of unity. Inner dimensions are 144 x 12 x 200 mm^3 (*L,W,H*) and the vessel is flooded with argon before pouring in the GaInSn through a silicon tube and a funnel. It cannot be excluded that by doing so air is entrained into the melt but great caution was applied on this filling process. Afterwards, the container opening is covered with duct tape, which is a fast, cheap and reliable solution to protect the liquid from external influences. Air can leave the vessel through a small hole and a layer of inert gas forms above the

liquid metal which reduces the oxidation rate. This is important because the reaction of metallic components with oxygen, e.g. to GaO_2 ($\rho \approx 4770$ kg m^{-3}) or Ga_2O_3 ($\rho \approx 6440$ kg m^{-3}) as depicted by Brito et al. [27], can change the composition of the liquid metal. Pure argon (Linde HIQ 5.0) is injected in the middle of the vessel through the side wall. The center of the nozzle cross-section is 4.6 mm above the bottom plate (which serves as the coordinate reference). The gas injection system is similar to the setup of C. Zhang and consists of a gas flow controller (MKS 179AX21CS1BV) and non-wetted medical injection needles of different sizes (B. Braun Medical Inc.). The inner nozzle diameters are $D_i \approx 0.385, 0.565, 0.785$ mm and the outer diameters $D_a \approx 0.64, 0.82, 1.09$ mm, respectively. By the choice of sharpened nozzles the intensity of initial bubble deformation through pinch off is supposed to be reduced.

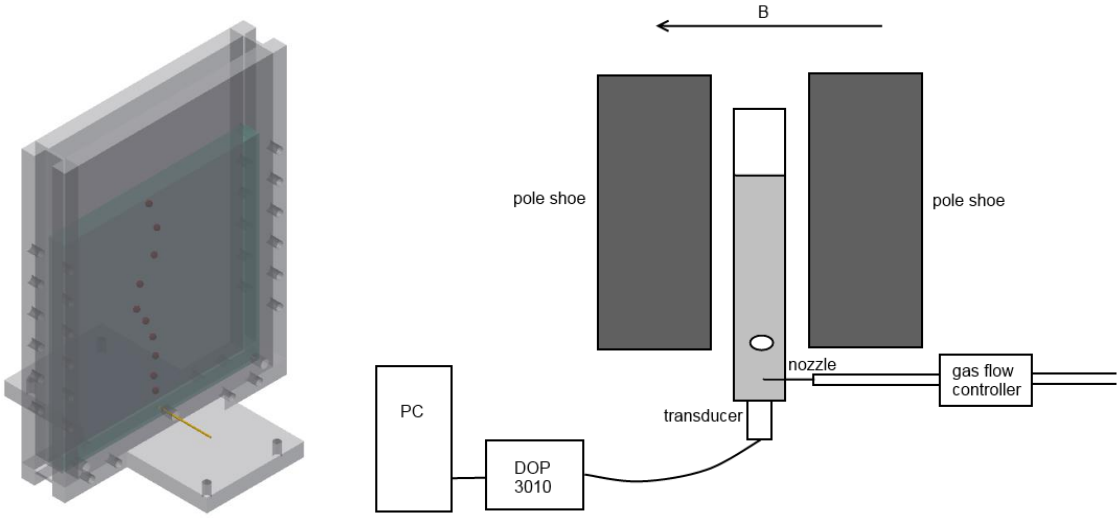

Fig. 1. Left: Model of the experiment (bubble chain as an illustration, holes in frame are to attach sensor from bottom or side, feet not displayed). Right: Simplified sketch of the electromagnetic setup.

The nozzle orifice is not oriented upwards but parallel to the bottom plate in order to define initial conditions. This increases reproducibility but also leads to a small shift of the bubble trajectory away from the centerline (see Richter et al. [25]). A detailed description of the detachment process becomes rather difficult and depends on many factors such as nozzle geometry, wetting conditions or gas flow rate ($\dot{m}$) which is chosen accordingly to the specific nozzle size between 12.67 and 36.17 mm^{3}s^{-1} to guarantee a single bubble regime. The influence of a previous bubble on the bubble rise cannot be completely neglected in the pure hydrodynamic system, but at higher magnetic fields as shown later on.

An electromagnetic system, consistent of a pair of Helmholtz coils with pole shoes made of stainless steel, is used to generate a uniform static magnetic field with magnetic flux densities up to $B \approx 0.918$ T. The magnetic field was measured with a 3 - axis Gauss meter (Lakeshore 460, sensor type MMZ-2512-UH) and is homogeneous within the volume between the pole shoes but shows a strong gradient along the rim. In Fig. 1 a sketch of the setup within the magnetic system is displayed. The homogeneous area of the magnetic field begins at a height of 10 mm which means that bubbles are subject to fringe field effects during formation and within the first moments of ascent. Irrespective of these effects, which cannot be quantified by UDV, the ascent of bubbles can be considered to occur fully within a homogeneous magnetic DC field.

2.1 Working liquid GaInSn

GaInSn is used in laboratory scale experiments because it is easy to handle and has moderate acquisition costs. It is less poisonous than mercury and liquid at room temperature. But unlike mercury GaInSn is not a noble metal and has a high reactivity with oxygen and aluminum. An overview of physical properties of GaInSn according to literature is presented in Table 2. The values differ,

especially the surface tension which affects the theoretical values for rise velocities or dimensionless numbers such as *Eo* or *We*.

Table 2. Physical properties of GaInSn according to literature. Not listed here is a study of Liu et al. [28] who experimentally determined the surface tension of GaInSn drops in nitrogen atmosphere to be $\sigma = 534.6 \pm 10.7$ mN m^{-1} at $T = 301.15$ K.

	Plevachuk et.al.2015 [29] [1]	Hodes et al. 2012 [30]	Morley et.al. 2008 [31]	Kocourek et al. 2006 [32]	Müller & Bühler 2001 [33]	C. Zhang 2005 & 2009 [2], [3]
ρ [kg/m³]	6360	6440	6360	6440	6363.2	6361
η [kg/m s]	2.09×10^{-3}	2.4×10^{-3}	$1.895 – 2.544 \times 10^{-3}$	-	2.215×10^{-3}	2.2×10^{-3}
σ [N/m]	0.587	0.535 – 0.718	0.533	0.718	-	0.533
σ_{el} [S/m]	3.26×10^{6}	3.3×10^{6}	3.1×10^{6}	3.46×10^{6}	3.307×10^{6}	3.27×10^{6}
T_M [°C]	10.55	-19	10.5	-	-	-
T_B [°C]	-	> 1300	> 1300	-	-	-
c [m/s]	-	-	2730	-	-	-

[1] Temperature dependent values are according to $T = 299$°K. Note that formula for density and thermal conductivity in Plevachuk et al. do not correspond to their experimental data.

Table 3, on the other hand, shows a chemical analysis of the metallic composition of the working liquid GaInSn used in this study. It is important to state that it is not the eutectic alloy $Ga^{67}In^{20.5}Sn^{12.5}$ and contains approx. 0.05 wt% other metals including traces of ferromagnetic metals Co, Ni, Gd and Dy. This deviation can be explained by the circumstance that the working liquid is regenerated chemically after usage with acid and heat. Here GaInSn is gathered from different experimental setups, where it has contact with other metals, and is processed afterwards. Because of this regeneration, on which the author has no influence, process parameters may change from one experimental campaign to another. Furthermore, the liquid cannot be considered as a homogeneous media. Local segregations (separate measurements with X-ray indicated that such phenomena can occur) may be of great importance. These segregations could result in a jump of the local physical properties such as electrical conductivity and acoustic impedance and could serve as “scattering particles” for the ultrasound measurement technique. In a study Borin et al. [34] claimed that an magnetic field changes the viscosity of GaInSn. The traces of ferromagnetic elements within the working liquid (Table 3) could also influence the rheology (e.g. Monajjemi Rarani et al. [35]) but these points have to be considered as unclarified.
C. Zhang, who worked at the same research facility as the author, did not mention the composition of GaInSn they used in their experiments. The author supposes that it also differed from the eutectic alloy since the regeneration procedure did not change basically within the last years. For the sake of comparability with experimental and numerical results, physical properties in this paper are those according to C. Zhang.

Table 3. Composition (metals) of working liquid GaInSn. Components Ga, In, Sn in wt%, all other values in µg/g. Metals with mass fractions below 0.1µg/g are not displayed. In comparison, eutectic alloy is $Ga^{67}In^{20.5}Sn^{12.5}$ in wt%.

Ga	68.40 wt%	**In**	23.33 wt%	**Sn**	8.22 wt%			
Pb	**K**	**Cu**	**Hg**	**Zn**	**Bi**	**Ni**	**Ba**	**Al**
189.4	53.0	48.9	43.9	35.3	17.2	12.0	8.2	7.5
Ag	**Mg**	**Co**	**Sb**	**Cs**	**Cr**	**Sr**	**Ce**	**Ge**
4.7	4.0	2.3	1.3	0.4	0.4	0.3	0.3	0.3
Gd	**Ti**	**Rd**	**W**	**Dy**	**La**	**Pr**		
0.3	0.2	0.2	0.2	0.1	0.1	0.1		

2.2 Measurement technique & signal processing

As in the studies of C. Zhang and Wang et al. [24] the Ultrasound Doppler Velocimetry (UDV) is used to investigate the ascent of bubbles in opaque liquid metal. UDV is a pulse-echo method which yields space-time resolved velocities of reflectors through a correlation algorithm between several emitted

and detected ultrasonic pulses (e.g. Kasai et al. [36], Müller-Stüler [37]). The applicability on the problem of two phase flows was investigated by several authors (e.g. Murakawa et al. [38], Murai et al. [39]) who state that, if the bubble is smaller or larger than the wavelength of the ultrasonic burst, this technique is practicable. A rectangular ultrasonic transducer (Richter Sensor & Transducer Technologie) with a transmitting area of 5 x 5.3 mm² is attached to the 2 mm thick wall below the nozzle and ultrasound bursts of 8 MHz are transmitted through a coupling gel to the liquid. It takes a bubble approximately half a second to rise from the nozzle to the free surface. Therefore pulse repetition intervals and amount of correlated echo signals are chosen to be low. The commercial device DOP 3010 (Signal Processing) is used for data processing which provides instantaneous (vertical) velocity profiles along the measurement path with a space-time resolution of approx. 10 ms per profile and 2.7 mm per height step, respectively. To achieve precise results by this device a precise knowledge of the speed of sound of the working liquid is essential. As already mentioned in the previous subchapter, the physical properties are not known exactly and are probably modified in an unpredictable way by microbubbles, local segregations or even oxide particles. To avoid these uncertainties, just the time span between bubble detachment and reaching the surface (basically the same technique used by Mori) is considered to evaluate the ascent velocities. The presented data are averaged values for at least 16 bubbles at each specific magnetic flux density (see appendix for amount and standard deviation).
The presented velocities contain an acceleration phase (short period after bubble detachment with fringe field effects), the ascent in quasi-steady state (where more or less periodic velocity oscillations may occur) and a (short) deceleration phase ahead of the free surface. In contrast, the velocity data given by C. Zhang represents mean terminal rise velocities without acceleration or deceleration phase. The UDV technique is not able to determine important features such as bubble shape, volume or intensity of gas circulations within the bubbles. An equivalent bubble diameter is derived from the gas flow rate for each experimental campaign, as proposed by C. Zhang. The equivalent diameter (d_{eq} [mm]) refers to a sphere of equal volume and is calculated from the gas flow rate ($\dot{m}$ [mm s^{-1}]) and the mean bubble detachment frequency (f [s^{-1}]).

$$d_{eq} = \sqrt[3]{\frac{6}{\pi}\frac{\dot{m}}{f}} \tag{1}$$

3 Experimental results & discussion

Wu & Gharib [40] and Tomiyama et al. [41] showed that the initial bubble deformation at the nozzle has a significant influence on the bubble behavior[1]. In general, a small bubble deformation leads to lower, large bubble deformation to higher rise velocities. In other words, a bubble of unhindered oscillation can be characterized by the well-known Mendelson equation Eq. (2) whereas bubbles of hindered oscillation, whether by low initial deformation or the presence of surface active substances ("contaminated liquid"), would behave more like a rigid sphere.

$$u_{Mendelson} = \sqrt{\frac{2\sigma}{\rho d_{eq}} + \frac{g d_{eq}}{2}} \tag{2}$$

In 1967, Mendelson [42] applied the wave theory of Lamb [43] to empirical data provided by Haberman & Morton [44] and showed that the rise velocity of (oscillating) bubbles in pure water correlates with the travelling velocity of surface waves.

[1]: To the contrary, deVries et al. [45] induced shape oscillations to bubbles in ultra-clean water by contact with a hot-film anemometer. Although an increasing trend of velocity is visible after the contact (see e.g. Fig. 2 in the corresponding paper), they concluded that shape oscillations do not affect the terminal ascent velocity.

Although no physical explanation was given (as noted by Maneri & Mendelson [46], Fan & Tsuchiya [47], Baz-Rodríguez et al. [48], Lehrer [49]) this equation fits experimental data well and the terminal rise velocity solely depends on the sphere equivalent bubble diameter (d_{eq}), surface tension (σ), liquid density (ρ) and gravitational acceleration (g), but not on other factors such as trajectory or bubble shape. The local minimum (Fig. 2) is achieved when the first term (surface tension dominant regime) and second term (gravitational force dominant regime) are equal; in non-dimensional form at Eo = 4. Several authors (e.g. Fan & Tsuchiya [47], Baz-Rodríguez et al. [48], Jamialahmadi [50], Tomiyama [41]) proposed equations to unify the rise velocity of small bubbles (which follow Stokes law) and large bubbles (where surface tension and/or inertia are predominant) considering the effect of surfactants. Most of these are parameter fits but no general equation is available for bubbles of low initial deformation or in contaminated media, where the terminal rise velocity is lower than in pure ones (e.g. Krzan & Malysa [51]). Next, the ascent velocities from literature will be compared and discussed with the present study at zero magnetic flux density. For a better overview this is subdivided into an experimental part (subchapter 3.1) with focus on the data provided by Mori and C. Zhang and a numerical part (subchapter 3.2) with data from Schwarz & Fröhlich [19] ("Schwarz") and J. Zhang et al. [20], [21] ("J. Zhang"). Afterwards (subchapter 3.3), the present study is compared with experimental and numerical results under the influence of a static magnetic field.

3.1 Comparison with experimental studies at zero magnetic flux density

The mean-averaged ascent velocities of single bubbles of different studies are compiled in Fig. 2. Experimental data of Mori (N_2 in mercury - blue circles) scatters around the theoretical value (blue line) but agrees well qualitatively and indicates that the Mendelson equation Eq. (2) is valid not only for pure water but for clean liquids in general. The data of C. Zhang shows an offset of approximately 15% from the theoretical value of GaInSn (red line), whereas the present study (black squares) seems to be in qualitative agreement with a "contaminated system" as depicted e.g. in Clift, Grace, Weber [52] (see Fig. 7.3, p. 172) Based on the assumption that the used GaInSn is of similar composition as that of C. Zhang, this indicates that bubbles of the present study are injected with low initial shape deformation and therefore behave more like "rigid spheres". Apart from the qualitative difference in trend, a fair agreement is achieved in rise velocity for bubbles of $d_{eq} \approx 4$ - 5.5 mm. Note that the slightly higher rise velocity at $d_{eq} \approx 5.074$ mm is related to a higher gas flow rate used. That is to show that bubbles which are affected by the wake of a previous bubble rise faster than bubbles in a quiescent liquid. That effect becomes negligible at higher magnetic flux densities (Fig. 4).

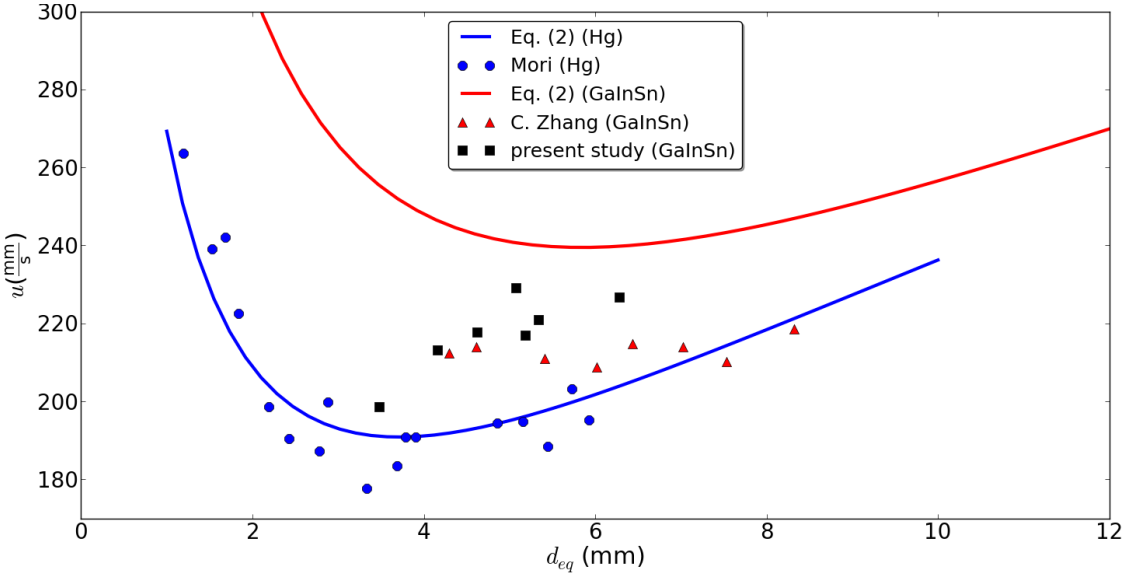

Fig. 2. Comparison of mean rise velocities of the present study (Ar - GaInSn: black squares with d_{eq} = 3.478, 4.155, 4.617, 5.074, 5.281, 5.334, 6.280 mm and Eo = 1.42, 2.03, 2.50, 3.01, 3.14, 3.33, 4.62, respectively) with data of Mori (N_2 - Hg: blue circles) and C. Zhang (Ar - GaInSn: red triangles) and the corresponding theoretical values according to Mendelson equation (2) (N_2 - Hg: blue line, Ar - GaInSn: red line) at zero magnetic field.

The main difference between the setup of C. Zhang (as well as that of Mori) and the present study is that they used a cylindrical vessel with a larger distance between bubbles and wall. One would expect that in a close confinement the rise velocity should be lower than in the case of free rise (Uno & Kintner [53], Maneri & Mendelson [46]), but for bubble sizes larger than d_{eq} ≈ 4.5 mm this is not the case, compared with the results of C. Zhang. A conclusive explanation on the difference in the deviating trends cannot be given at this point.

3.2 Comparison with numerical data at zero magnetic flux density

In this subchapter, the mean-averaged ascent velocities are compared with numerical results. Here, as in Fig. 2, black squares indicate data from the present study whereas green and yellow symbols represent data from J. Zhang and Schwarz, respectively. J. Zhang simulated the setup argon & GaInSn (same physical properties as in C. Zhang) by means of the volume-of-fluid method (VOF) with an adaptive mesh refinement (AMR) solving the incompressible Navier-Stokes equations with a Lorentz force (in case of magnetic field) and surface tension force term, considering also the Marangoni effect. The bubbles were simulated with spheroidal shape at initial conditions and accelerated due to buoyancy before reaching a stable state. The domain was (L,W,H) = 20 d_{eq} x 20 d_{eq} x 40 d_{eq} and large enough to safely ignore wall effects.

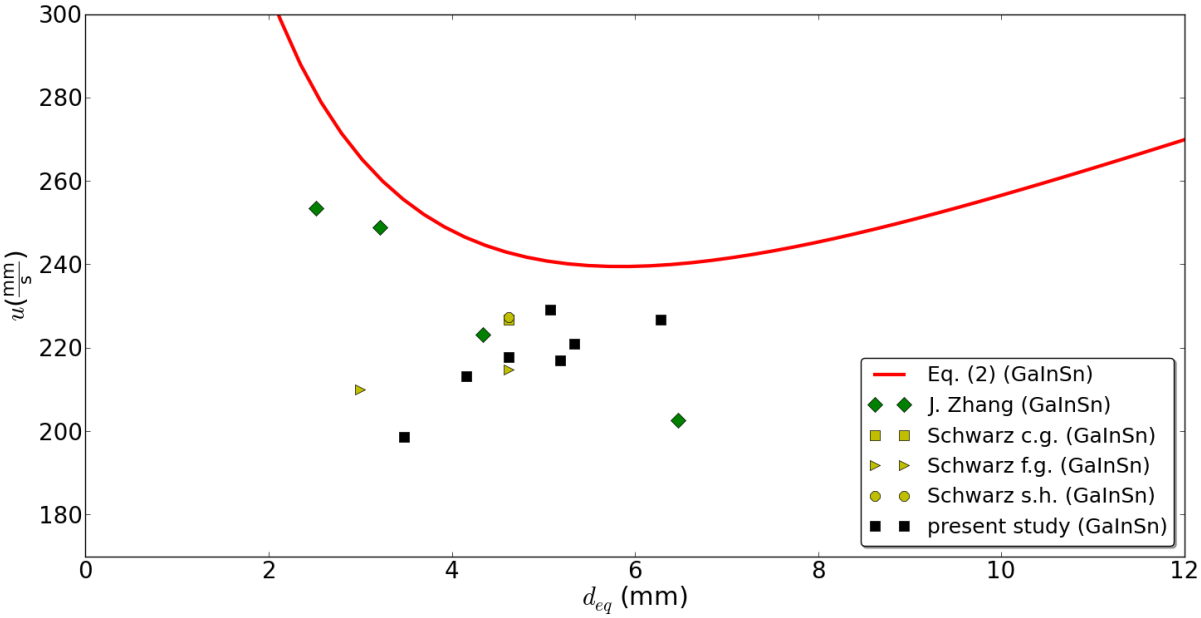

Fig. 3. Comparison of mean rise velocities of present study (Ar - GaInSn: black squares) with data of Schwarz (Ar - GaInSn: yellow markers) and J. Zhang (Ar - GaInSn: green diamonds) and the corresponding theoretical values according to Mendelson equation (2) (Ar - GaInSn: red line) at zero magnetic field. (f.g. - fine grid, c.g. - coarse grid, s.h. - spherical harmonics)

The numerical velocities of J. Zhang (green diamonds) are in qualitative agreement with the theoretical value (red line) but bubbles are slower. In case of d_{eq} = 6.47 mm the obtained velocity (u_T = 202.7 mm s^{-1}) does not fit the theoretical value nor the experiments of either C. Zhang (d_{eq} ≈ 6.44 mm, u_T ≈ 214.7 mm s^{-1}) and the present study (d_{eq} ≈ 6.28 mm, u_T ≈ 226.7 mm s^{-1}). On the other hand, the rise velocity of a d_{eq} = 4.34 mm bubble with u_T ≈ 223.1 mm s^{-1} is in general agreement with experimental data (C. Zhang: d_{eq} ≈ 4.30 mm, u_T ≈ 212.5 mm s^{-1}; present study: d_{eq} ≈ 4.17 mm, u_T ≈ 213.2 mm s^{-1}) and numerical results of Schwarz. According to the data presented by J. Zhang the dependency of ascent velocity and bubble diameter seems almost linearly, inversely proportional. This is in contrast to experimental observations and theoretical considerations. Schwarz investigated the rise of argon bubbles (d_{eq} = 4.60 mm) in GaInSn (same physical properties as in C. Zhang) within a domain of (L,W,H) = 6d_{eq} x 6d_{eq} x 30d_{eq} by means of VOF. Bubbles are spherical at initial conditions and the bubble surface is represented by an immersed boundary method with no slip condition. The shape of the bubble is approximated by an ellipsoid with an axis ratio X derived from the instantaneous Weber

number according to Loth [54] with $X^{-1}(t) = 1 - 0.75 * \tanh(0.165 * We(t))$. Schwarz used two different spatial resolutions of the Eulerian grid with n = 265, called “fine grid” (f.g. - yellow triangles) and n = 192, called “coarse grid” (c.g. - yellow squares). As shown in Fig. 3 both calculated velocities agree well with the experimental data. In the case of the “fine grid”, the numerical value (u_T = 214.8 mm s^{-1}) is closer to the experimental data (C. Zhang: $d_{eq} \approx$ 4.61 mm, $u_T \approx$ 213.9 mm s^{-1}; present study: $d_{eq} \approx$ 4.62 mm, $u_T \approx$ 217.8 mm s^{-1}) than the value for the “coarse grid” (u_T = 226.7 mm s^{-1}). Additionally, they run simulations with bubble shapes represented not by ellipsoids but with by axisymmetric spherical harmonics (s.h. - yellow circles). This result ($u_T \approx$ 227.3 mm s^{-1}) is almost identical with the “coarse grid” value.

3.3 Comparison with results under the influence of a magnetic field

In Fig. 4 the ascent velocity for different bubble sizes are depicted in dependence of the magnetic flux density (B). Typically, three different effects are observed. The bubble rise is retarded at lower, accelerated at moderate and finally dampened at high magnetic fields. The maximal velocity of larger bubbles is reached at lower flux densities than of smaller bubbles. The difference in rise velocity of bubbles with Eo (B = 0 T) = 3.01 and 3.14 is due to a higher gas flow rate at former experiment ($\dot{m}$ = 36.17 and 12.67 mm^3 s^{-1}, respectively). Although still in the single bubble regime, the induced flow influences the following bubble. This “slipstream” effect is negligible at higher magnetic flux densities and local maxima of both cases can be found at approximately the same point. This strongly indicates that the bubble wake and global re-circulations are suppressed by the magnetic field as already mentioned by Schwarz, J. Zhang and C. Zhang.

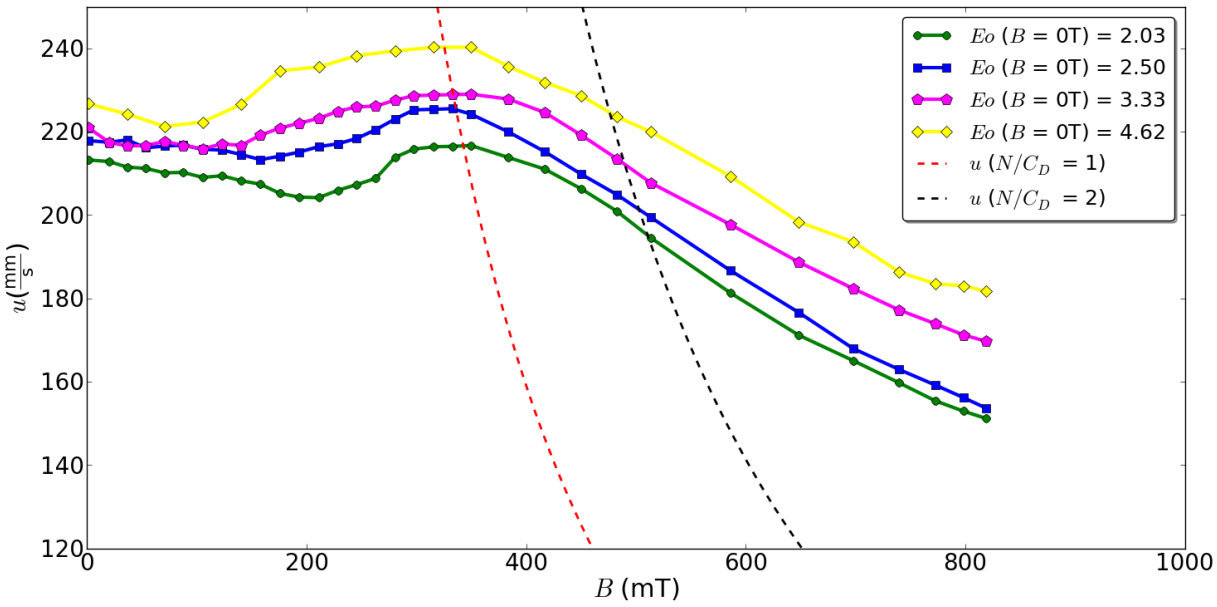

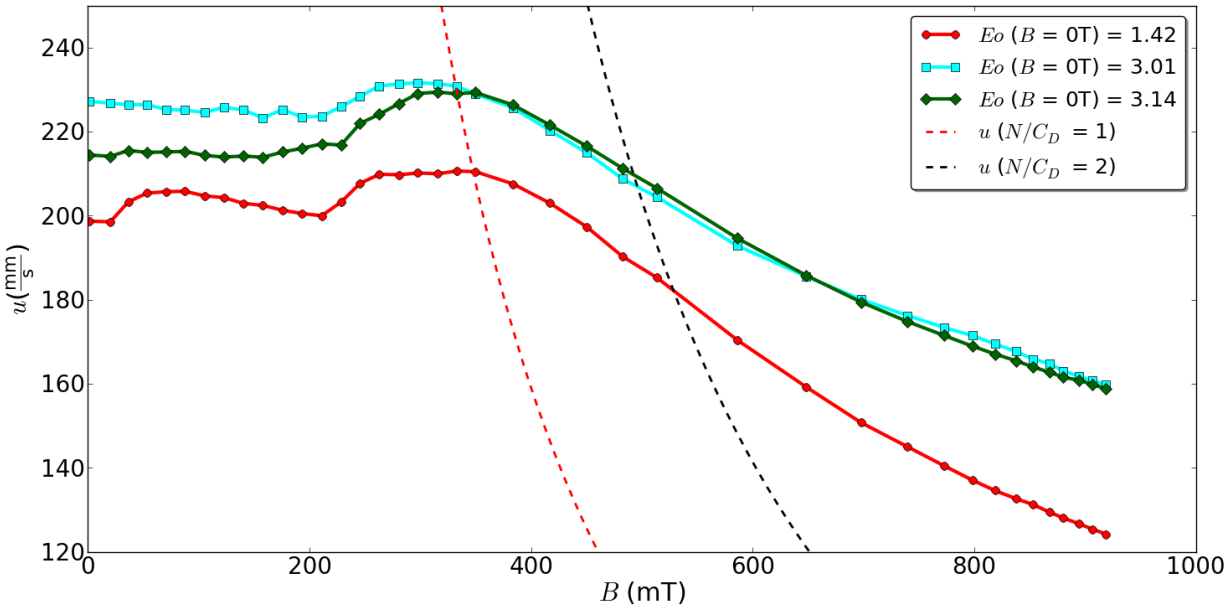

Fig. 4. Mean rise velocity in dependence of magnetic flux density for bubbles of different sizes. *Eo* numbers are given for mean bubble size at zero magnetic field. Local maxima and inclination points are approximately at $N/C_D = 1$ and $N/C_D = 2$, respectively and are shown as dashed lines. Number of averaged bubbles per data point and standard deviations can be found in the appendix.

In their paper considering a VMF, J. Zhang defined a relationship between Lorentz and gravitational forces as $Eo_m/Eo = \sigma_{el} u B^2/\Delta\rho g$ and stated that for bubbles larger than $Eo = 0.74$ the maximum velocity is reached when $Eo_m/Eo \approx 1.14$. According to the present data a maximum can be seen at $N/C_D \approx 1$ (which would be equal to $Eo_m/Eo = 4/3$), as shown in Fig. 4 with

$$\frac{N}{C_D} = \frac{3}{4}\frac{\sigma_{el} B^2 u}{\Delta\rho g} \tag{3}$$

where N refers to the Stuart number and C_D to the drag coefficient.

A relation of those two forces seems to be a suitable parameter to characterize the behavior of ascending bubbles under the influence of a magnetic field, since buoyancy is the driving force and motion of an electrically conducting liquid is modified by magnetic fields. As suggested by Schwarz and J. Zhang this accelerating effect seems to be related to the reduction of vorticity at the bubble surface and in the wake due to the acting Lorentz forces. A suppression of path instabilities is observed (not depicted here) for all d_{eq} studied. This could be the result of a general laminarization of the flow. The specific flux density at which the bubble path is rectilinear seems to correlate with the inclination point of the graphs at higher field strengths (as indicated by the results of Richter et al. [25]). These inclination points can be approximated with $N/C_D \approx 2$ and at magnetic flux densities greater than that value the declination of velocity seems to behave asymptotically. That agrees well with the findings of Wang [24]. For the studied bubble sizes the magnetic flux density of the inclination point is approximately 1.5 times the flux density of the maximum. In summary, this means that the steady state force balances at maximum and inclination point seem reduce to the simple form of $N/C_D \approx 1$ and $N/C_D \approx 2$, respectively. Additionally, the relationship between maximal rise velocity u_{max} and rise velocity at the inclination point u_{incl} can be approximated with $u_{max} \approx 1.125\, u_{incl}$ (from $B_{incl} \approx 1.5\, B_{max}$ in Eq. (3)). It is worth to note that these specific velocities seem to be independent of surface tension.
In general, it is likely that the influence of a magnetic field also affects surface oscillations, bubble shape and bubble-surfactant interaction. Within the present study, the bubble sizes vary with magnetic flux density as shown in Fig. 5, which seems to be related to the bubble formation process within the fringe field. An almost linear inclination of the diameter is recognized with increasing field strengths for almost all experiments. But for $B < 0.1$ T the behavior seems to depend on many factors such as the nozzle geometry or size. The inclination for $B > 0.1$ T can be related to a retarding effect caused by

the Lorentz force in such way that a higher gas volume is necessary to generate enough buoyancy for pinch off. The data indicates that smaller bubbles are less affected than larger bubbles.

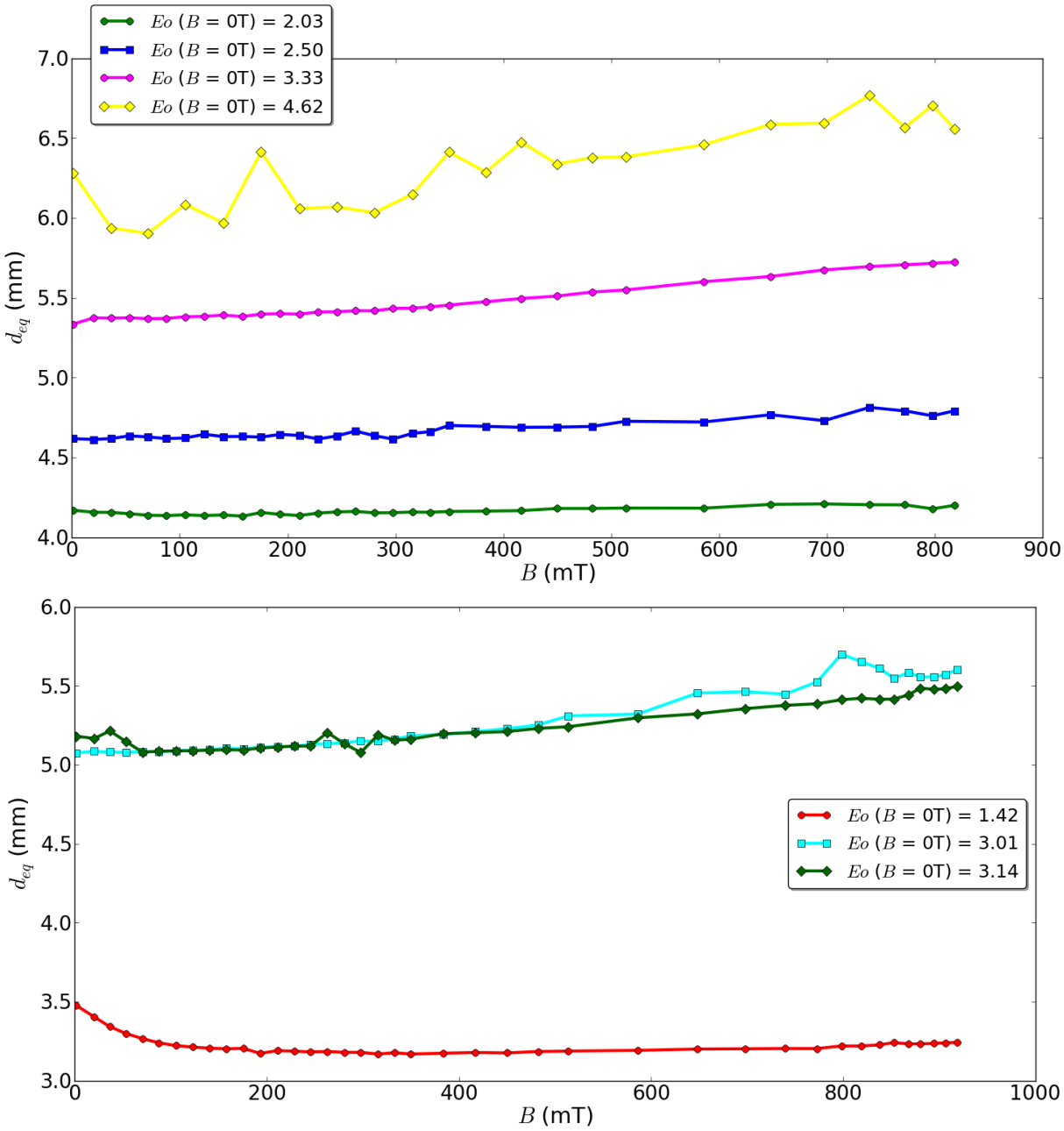

Fig. 5. Mean, sphere equivalent bubble diameter in dependence of magnetic flux density for bubbles of different sizes. *Eo* numbers are given for mean bubble size at zero magnetic field. Number of averaged bubbles per data point and standard deviations can be found in the appendix.

A comprehensive comparison with the data of C. Zhang is difficult because their experimental setup was limited to magnetic flux densities of approximately $B \approx 0.3$ T. As seen in Fig. 4 maximal velocities are achieved in that region. Additionally, their bubbles (as well as those of Mori) were generated far away from the magnetic pole shoes, rose unhindered towards the magnetic fringe and were then subject to a positive flux density gradient. According to Ishomoto et al. [6], such fringe field effects lead to a deceleration of the rise velocity and an elongation of the bubble shape along the magnetic field direction. To this point, based on their data, the influence of fringe field effects remains unclarified. An overview of the total rise velocities of Mori at different magnetic flux densities is given in Fig. 6. Qualitatively they showed that bubbles smaller than $Eo = 4$ (which is the local minimum of the Mendelson equation) experience an acceleration at medium magnetic flux densities and bubbles with $Eo > 4$ are purely decelerated under the influence of a magnetic field. The direct effect of a

homogeneous magnetic field on the velocity is shown in Fig. 7. Here *U'* is the velocity calculated between the lower and upper electrode of the electrical triple probe (see fig. 9 in the corresponding paper) and therefore this value should represent the vertical bubble velocity without path influence. The solid lines in Fig. 7 are 3rd order polynomial fits of the data presented by Mori with:

$$U = -54.66B^3 + 77.21B^2 - 0.534B + 186.92 \quad (4)$$

$$U' = -100.61B^3 + 163.09B^2 - 70.23B + 275.83 \quad (5)$$

The theoretical maximum (N/C_D = 1) and the theoretical inclination point (N/C_D = 2) for mercury are presented as dashed lines. In general, the rise velocities measured between the probe electrodes U' (green line: U' = 275.83 mm s^{-1} at B = 0 T) are much higher than the values obtained from the traveling time between the nozzle and the probe (blue line: U = 186.92 mm s^{-1} at B = 0 T). According to Mori the difference is due to a spiraling motion of the bubbles. Nevertheless, the data of *U'* indicates that a strong decelerating effect takes place for B > 1 T and the data of U shows qualitatively the same behavior as the curves of the present study with a local maximum at N/C_D = 1 (Fig. 4). There is no data for *U'* at B ≈ 1 T to verify if the acceleration is truly related to the suppression of path instabilities or if other effects such as shape elongation are crucial. If the assumption is correct that the acceleration effect is merely a straightening of the bubble trajectory due to a reduction of vorticity, an acceleration effect should not be visible for bubbles which already rise on a rectangular path, such as very small or very large bubbles. The experiments of Mori indicate that this could be the case but is not observed here because of the limitation of bubble sizes smaller than Eo ≈ 4.

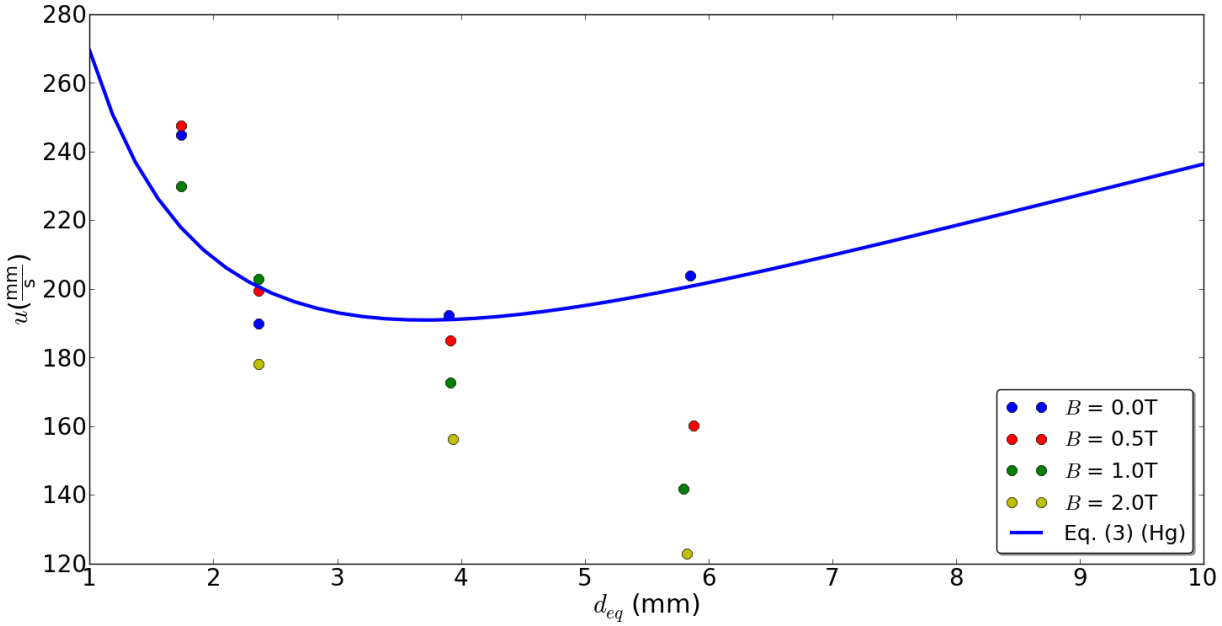

Fig. 6. Mean rise velocity of N_2 bubbles in mercury at different magnetic flux densities (B = 0 T: blue, B = 0.5 T: red, B = 1.0 T: green, B = 2.0 T: yellow) according to Mori. In comparison to small bubbles with Eo < 4 (local minimum of Mendelson equation (1) data indicate that bubbles with Eo > 4 are not accelerated at medium flux densities.

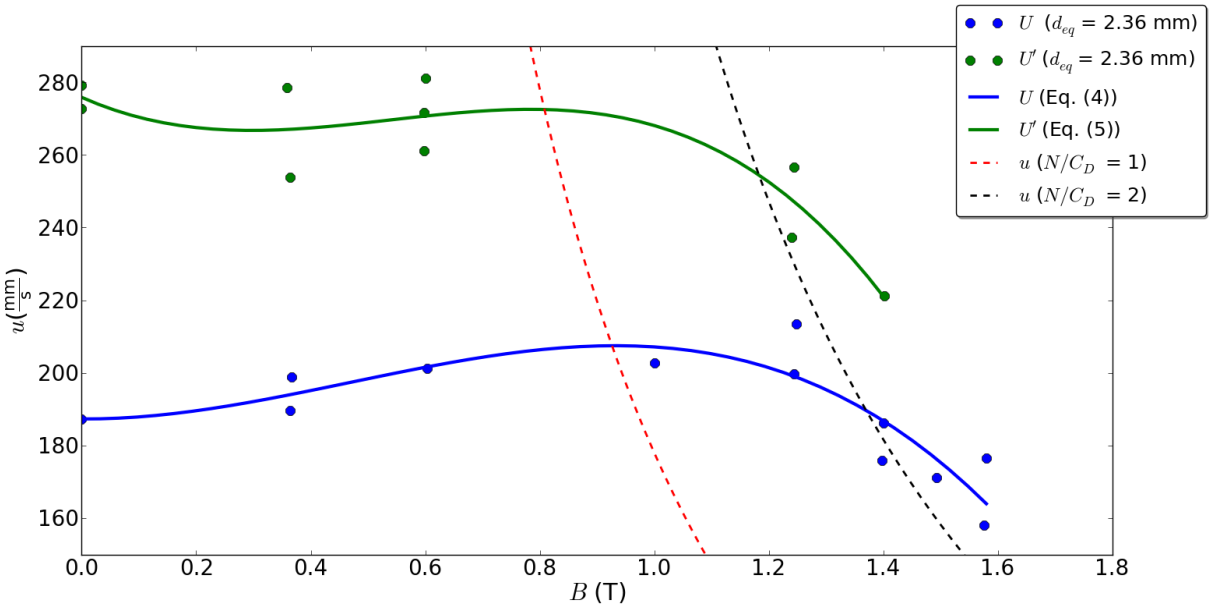

Fig. 7. Mean rise velocity (from nozzle to triple probe – blue circles) of bubble d_{eq} = 2.36 mm (*Eo* = 1.62) according to Mori (see Fig. 9 in the corresponding paper) and rise velocity (from lower to upper electrode of triple probe - green circles). Further shown are 3rd order polynomial fits (Eq. (3) for *U*: blue line and Eq. (4) for *U'*: green line) as well as theoretical, local maxima N/C_D = 1 and inclination point N/C_D = 2 (dashed lines) for system N_2-Hg.

Experimental results of C. Zhang and the present study are compared for similar bubble sizes under the influence of a HMF (Fig. 8) and a VMF (Fig. 9). As shown in Fig. 8 a good qualitative agreement is achieved but with an offset in total rise velocity. A reduction at low, as well as an increase at medium magnetic flux densities is visible. The local minimum agrees well at small, but a deviation exists between the values at large bubble sizes. The theoretical maximum at N/C_D = 1 seems to be in agreement with the data of C. Zhang but is not reached due to the limitation of their setup to $B \approx 0.3$ T.

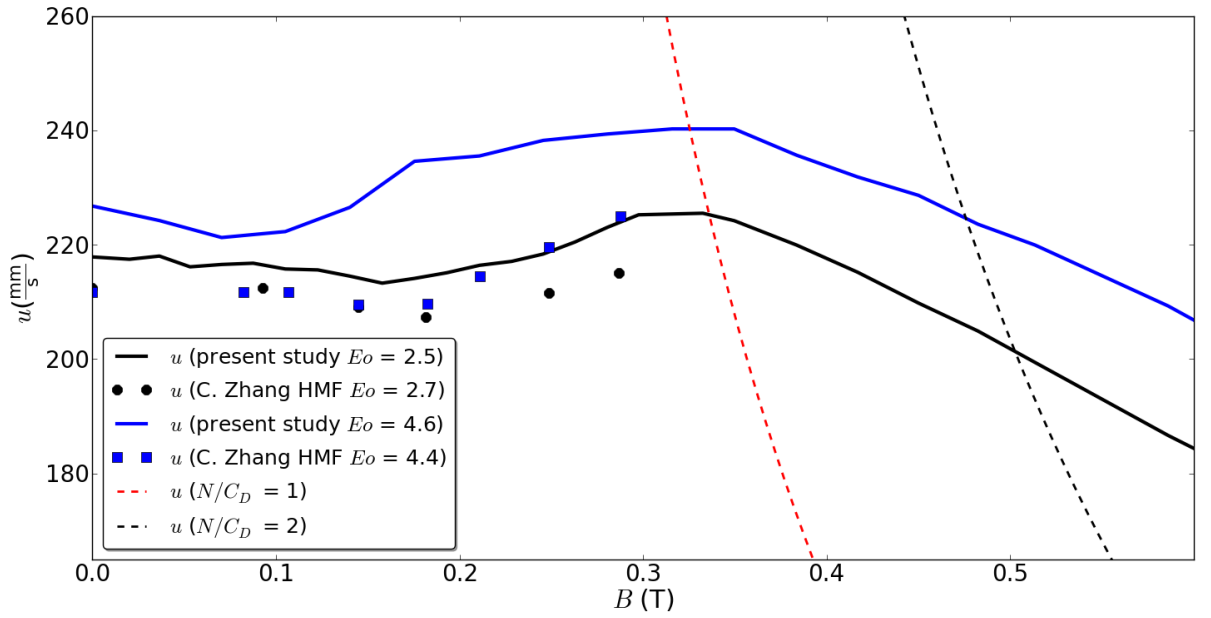

Fig. 8. Comparison of present study with similar data of C. Zhang for the HMF configuration. Local maxima at N/C_D = 1 as well as inclination point at N/C_D = 2 as dashed lines.

The comparison of this study (HMF) with C. Zhang (VMF) shows both differences and similarities. An accelerating effect is observed in VMF case (but at lower flux densities than with HMF) and larger bubbles seem to be more affected than smaller ones (Fig. 9). It seems that the general influence (acceleration at lower, deceleration at higher magnetic flux densities) is similar but not the same.

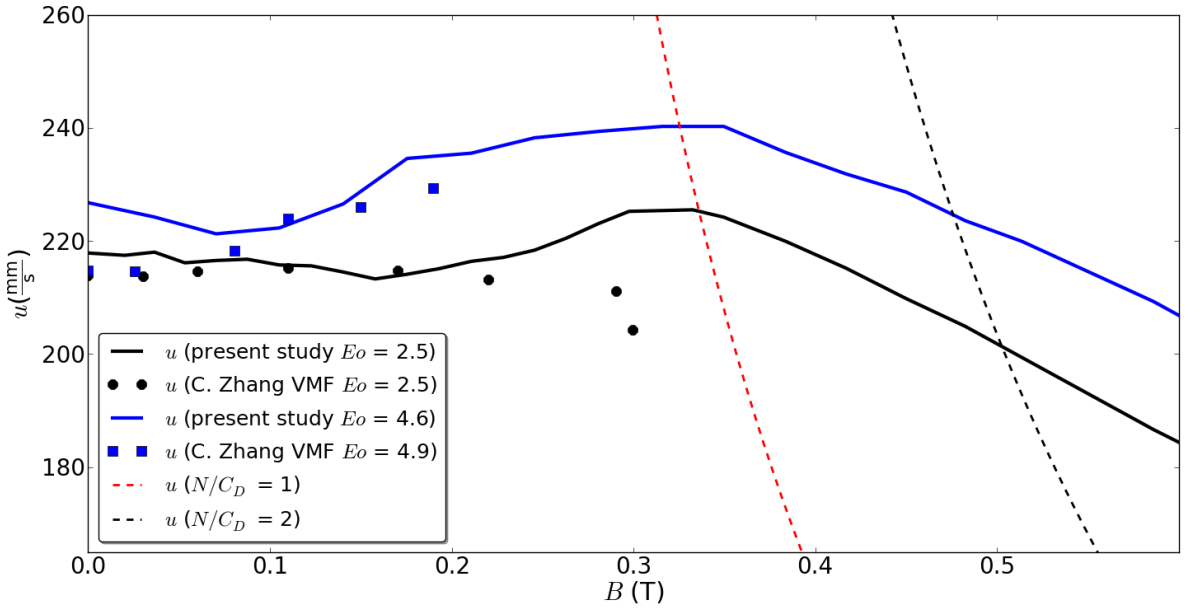

Fig. 9. Comparison of present study with similar data of C. Zhang for the VMF configuration. Local maxima at N/C_D = 1 as well as inclination point at N/C_D = 2 as dashed lines.

Finally, let us compare the present study with numerical simulations. To the knowledge of the author there are only three numerical investigations with the configuration Ar - GaInSn, namely those of Schwarz and J. Zhang who simulated the bubble ascent velocity under the influence of a VMF and J. Zhang dealing with the HMF configuration. Although the bubble sizes differ slightly (Schwarz: *Eo* = 2.5, J. Zhang: *Eo* = 2.2, present study: *Eo* = 2.5; or d_{eq} = 4.60, 4.30 and 4.62 mm respectively) the experiment and all numerical results are presented in Fig. 10. The data of Schwarz with VMF (bubble shape represented by spherical harmonics (s.h.)) are in qualitatively excellent agreement with the experiment (HMF). Also their data for the “coarse grid” (c.g.) and “fine grid” (f.g.) are in good agreement. The reasons why their code for VMF agrees that well with the experiments with HMF cannot be clarified at this moment. Note that Schwarz used the same electrical conductivity for gaseous- and liquid phase in case of “coarse grid” and “fine grid” calculations but an isolating bubble in case of “spherical harmonics”. On the other hand, numerical data of J. Zhang with VMF is in fair agreement with the present study but the local maximum is not predicted correctly at approximately half of the magnetic flux density of the experiment. J. Zhang presented a formula (5) (see Fig. 11 in [21]) for the rise velocity in dependence of the magnetic field and the rise velocity without applied magnetic field (u_0), valid for the HMF configuration and B > 0.3 T.

$$u = \left(1.3e^{-\left(\frac{B}{0.735\mathrm{T}}\right)} + 0.09\right) u_0 \qquad (5)$$

For *Eo* = 2.2, J. Zhang calculated a rise velocity u_0 = 223.126 mm s^{-1}. As seen in Fig. 10 there is a qualitative agreement but a large offset, moreover the local maximum is not predicted correctly. But the experimental results of this paper confirm the general form of Eq. (5) (see Eq.6).

$$u = \left(a * e^{-\left(\frac{B}{b}\right)} + c\right) u_0 \qquad (6)$$

Table 4 shows parameter for Eq. 6, Fig. 11 exemplary the original data and the fits for *Eo* = 2.03 and 2.50 because here the sphere equivalent diameter does not change much with increasing flux densities so that an empirical equation of u = f (B) seems justified. The most striking feature is that the dampening effect at high magnetic flux densities (where path instabilities are suppressed) seems to be an exponential function with u = f($e^{-(2B)}$). Moreover, the parameter c (which gives the asymptotic minimum at $B \rightarrow \infty$ with $u = c*u_0$) seems to be roughly 0.3…0.6 and is lower for small d_{eq}. That means that the asymptotic minimal velocities of the experiments (as well as those of Wang et al.) seem to be higher than $u = 0.09*u_0$, as predicted numerically by J. Zhang.

Table 4: Variables a, b and c for parameter fit according to Eq. 6 for different bubble sizes.

Eo (*B* = 0T)	*a* [-]	*b* [T]	*c* [-]
1.42	1.52	0.5	0.385
2.03	1.27	0.5	0.460
2.50	1.27	0.5	0.460
3.01	1.05	0.5	0.525
3.14	1.18	0.5	0.540
3.33	1.10	0.5	0.545
4.62	1.10	0.5	0.570

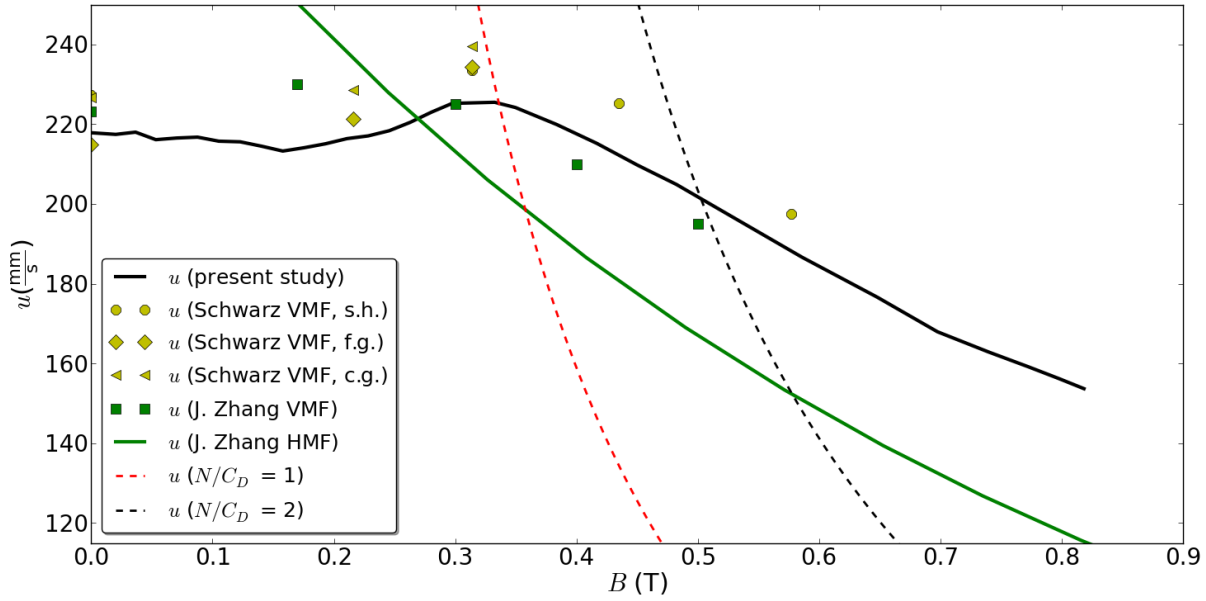

Fig. 10. Comparison of present study (HMF) with numerical results of Schwarz (VMF: yellow symbols with “coarse grid” – c.g., “fine grid” – f.g. and “spherical harmonics” – s.h.), J.Zhang (VMF: green squares) and J.Zhang (HMF: green line according to Eq. 5). Local maxima at N/C_D = 1 as well as inclination point at N/C_D = 2 are shown as dashed lines.

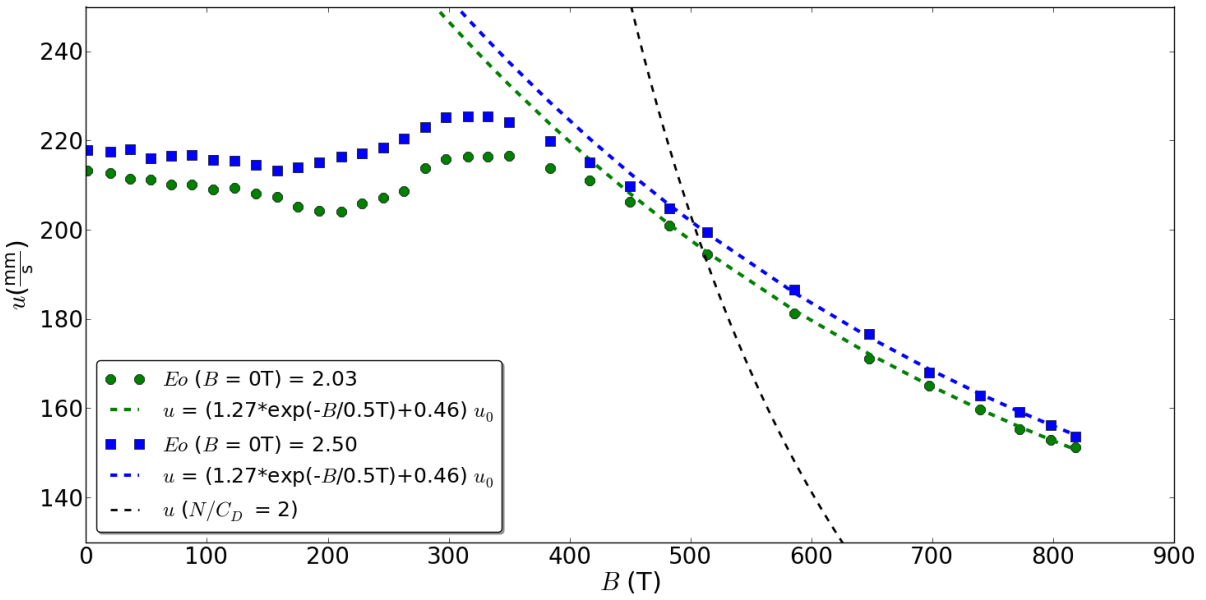

Fig. 11: Ascent velocities for *Eo* (*B* = 0T) = 2.03 and 2.50 with parameter fits according to Eq. 6 and Table 4. Inclination point (N/C_D = 2) as black dashed line.

4. Conclusions & Remarks

The ascent of single argon bubbles of sphere equivalent diameters between $d_{eq} \approx 3.43$ and 6.28 mm is investigated under the influence of a homogeneous, horizontal magnetic DC field in a flat, cubic vessel filled with GaInSn by means of UDV. Although the bubble diameter varies with magnetic field intensity it is shown that the ascent velocity is reduced at low, increased at medium and again reduced at high flux densities, compared to the case without a magnetic field. The maximum velocity seems to follow the simple relationship of $N/C_D \approx 1$ and the magnetic flux density at which the path instability vanishes, seems to correlate with $N/C_D \approx 2$. This agrees well with experimental data provided by Mori et al. [1], C. Zhang et al. [2], [3] and is in general agreement with the findings of Wang et al. [24]. Empirical equations are presented to fit the ascent velocities at higher magnetic flux densities. The declination seems to be a function $u = f(e^{-(2B)})$ and the asymptotic minimum seems to be approximately 30 to 60% of the bubble rise velocity without magnetic field, which is more than predicted by J. Zhang. The conclusions of this paper should be considered as limited to the studied parameter range and it is likely that bubbles which already rise on a straight path (Taylor bubbles with $Eo >> 4$ or small spherical bubbles with $Eo << 1$) are only subject of a reduction of terminal velocity with increasing flux densities, as indicated by the results of Mori. A comprehensive comparison with numerical studies showed that the simulation of Schwarz & Fröhlich [19] with a VMF configuration agrees well with the experiments (in a close confinement) with HMF. Numerical results by J. Zhang et al. [20], [21] with HMF show differ largely from the experiments. In contrast to the findings of Schwarz & Fröhlich, their simulations with VMF configuration does not agree with the experimental results. Moreover, their calculated velocities without a magnetic field do not fit experimental or theoretical results at higher d_{eq}. The reasons for this cannot be clarified at this moment. Data of this study as well as the recalculated results of the corresponding paper are given in the appendix for a better comparison. The investigation of smaller and larger bubbles as well as a configuration with VMF should be the following steps to verify the conclusions of this paper.

The author

Erik Strumpf graduated as a process engineer from Technical University Magdeburg, Germany and currently works as a research assistant at Helmholtz Center Dresden Rossendorf (HZDR), Germany.

Tel: +49 351 260 3031, Mail: e.strumpf@hzdr.de

Acknowledgements

The author likes to thank Marco Starace for helpful advices.

Literature

[1] Y. Mori, K. Hijikata and I. Kurlyama, “Experimental Study of Bubble Motion in Mercury With and Without a Magnetic Field,” *J. Heat Transf.*, vol. 3, no. 99, pp. 404–410, 1977.

[2] C. Zhang, S. Eckert and G. Gerbeth, “Experimental study of single bubble motion in a liquid metal column exposed to a DC magnetic field,” *Int. J. Multiph. Flow*, vol. 31, no. 7, pp. 824–842, Jul. 2005.

[3] C. Zhang, “Liquid Metal Flows Driven by Gas Bubbles in a Static Magnetic Field”, Technische Universität Dresden, Dresden, 2009.

[4] K. Jin, P. Kumar, S. P. Vanka, and B. G. Thomas, “Rise of an argon bubble in liquid steel in the presence of a transverse magnetic field,” *Phys. Fluids*, vol. 28, no. 9, p. 93301, Sep. 2016.

[5] K. Ueno, M. Higashitani and S. Kamiyama, “Study on single bubbles rising in magnetic fluid for small Weber number,” *J. Magn. Magn. Mater.*, vol. 149, no. 1, pp. 104–107, 1995.

[6] J. Ishimoto, M. Okubo, S. Kamiyama and M. Higashitani, “Bubble Behavior in Magnetic Fluid under a Nonuniform Magnetic Field,” *JSME Int. J.*, vol. 3, no. 38, pp. 382–387, 1995.

[7] K. Ueno, T. Nishita, and S. Kamiyama, “Numerical simulation of deformed single bubbles rising in magnetic fluid,” *J. Magn. Magn. Mater.*, no. 201, pp. 281–284, 1999.

[8] K. Nakatsuka, B. Jeyadevan, Y. Akagami, T. Torigoe and S. Asari, “Visual observation of the effect of magnetic field on moving air and vapor bubbles in a magnetic fluid,” *J. Magn. Magn. Mater.*, vol. 201, pp. 256–259, 1999.

[9] T. Tagawa, “Numerical simulation of two-phase flows in the presence of a magnetic field,” *Math. Comput. Simul.*, vol. 72, no. 2, pp. 212–219, 2006.

[10] G. Huang, R. Hong, H. Li and J. Ding, “Experimental and numerical investigations of rising gas bubble with different initial shape in a magnetic fluid,” *Comput. Appl. Chem.*, vol. 25, no. 6, pp. 641–644, 2008.

[11] D. Merrouche, K. Mohammedi and I. Belaidi, “Coupling the VOF and the MHD models for the simulation of bubble rising in a metallic liquid,” *Int. J. Mater. Form.*, vol. 1, no. S1, pp. 1107–1110, Apr. 2008.

[12] M. S. Korlie, A. Mukherjee, B. G. Nita, J. G. Stevens, A. D. Trubatch and P. Yecko, “Modeling bubbles and droplets in magnetic fluids,” *J. Phys. Condens. Matter*, vol. 20, no. 20, p. 204143, May 2008.

[13] D. Gaudlitz and N. A. Adams, “The Influence of Magnetic Fields on the Rise of Gas Bubbles in Electrically Conductive Liquids,” in *Direct and Large-Eddy Simulation VII*, Trieste, Italia, 2010, vol. 13, pp. 465–471.
[14] Y. Shibasaki, K. Ueno and T. Tagawa, “Computation of a rising bubble in an enclosure filled with liquid metal under vertical magnetic fields,” *ISIJ Int.*, vol. 50, no. 3, pp. 363–370, 2010.
[15] K. Kumazawa, I. Furuhashi and K. Iwai, “Effect of Horizontal Static High Magnetic Field on Velocity of Single Bubble Rising in Saturated Sodium Chloride Solution,” *J. Jpn. Soc. Exp. Mech.*, vol. 10, no. 2, pp. 198–202, 2010.
[16] Y. Pan and M.-J. Ni, “Numerical simulation of bubble rising in conductive liquids under magnetic field,” *J. Eng. Thermophys.*, vol. 33, no. 1, pp. 75–78, 2012.
[17] M. R. Ansari, A. Hadidi and M. E. Nimvari, “Effect of a uniform magnetic field on dielectric two-phase bubbly flows using the level set method,” *J. Magn. Magn. Mater.*, vol. 324, no. 23, pp. 4094–4101, Nov. 2012.
[18] J. Zhang and M.-J. Ni, “Direct simulation of multi-phase MHD flows on a unstructured Cartesian adaptive system,” *J. Comput. Phys.*, vol. 270, pp. 345–365, 2014.
[19] S. Schwarz and J. Fröhlich, “Numerical study of single bubble motion in liquid metal exposed to a longitudinal magnetic field,” *Int. J. Multiph. Flow*, vol. 62, pp. 134–151, Jun. 2014.
[20] J. Zhang and M.-J. Ni, “Direct simulation of single bubble motion under vertical magnetic field: Paths and wakes,” *Phys. Fluids*, vol. 26, no. 10, p. 102102, Oct. 2014.
[21] J. Zhang, M.-J. Ni and R. Moreau, “Rising motion of a single bubble through a liquid metal in the presence of a horizontal magnetic field,” *Phys. Fluids*, vol. 28, no. 3, p. 32101, Mar. 2016.
[22] X.-H. Tian, W.-Y. Shi, T. Tang, and L. Feng, “Influence of Vertical Static Magnetic Field on Behavior of Rising Single Bubble in a Conductive Fluid,” *ISIJ Int.*, vol. 56, no. 2, pp. 195–204, 2016.
[23] H. Yamasaki and H. Yamaguchi, “Numerical simulation of bubble deformation in magnetic fluids by finite volume method,” *J. Magn. Magn. Mater.*, Oct. 2016.
[24] Z.-H. Wang, S.-D. Wang, and M.-J. Ni, “The experimental study of Ar bubble rising in liquid metal under strong magnetic field,” *Int J Heat Mass Transf.*, 2016.
[25] T. Richter, O. Keplinger, E. Strumpf, T. Wondrak, K. Eckert, S. Eckert and S. Odenbach, “Measurements of the diameter of rising gas bubbles my means of the Ultrasound Transit Time Technique,” *10th PAMIR Int. Conf. - Fundam. Appl. MHD*, submitted.
[26] K. Iwai and I. Furuhashi, “Bubble Rising Velocity in Sodium Chloride Aqueous Solution under Horizontal DC High Magnetic Field,” in *5th International Workshop on Complex Systems*, Sendai, Japan, 2008, vol. 1, pp. 654–657.
[27] D. Brito, H.-C. Nataf, P. Cardin, J. Aubert and J.-P. Masson, “Ultrasonic Doppler velocimetry in liquid gallium,” *Exp. Fluids*, no. 31, pp. 653–663, 2001.
[28] T. Liu, P. Sen and C.-J. Kim, “Characterization of Nontoxic Liquid-Metal Alloy Galinstan for Applications in Microdevices,” *J. Microelectromechanical Syst.*, vol. 21, no. 2, pp. 443–450, Apr. 2012.
[29] Y. Plevachuk, V. Sklyarchuk, S. Eckert, G. Gerbeth and R. Novakovic, “Thermophysical Properties of the Liquid Ga–In–Sn Eutectic Alloy,” *J. Chem. Eng. Data*, vol. 59, no. 3, pp. 757–763, Mar. 2014.
[30] M. Hodes, R. Zhang, R. Wilcoxon and N. Lower, “On the Cooling Potential of Galinstan-Based Minichannel Heat Sinks,” presented at the 13th IEEE ITHERM Conference, Sheraton, San Diego, CA, USA, 2012, pp. 297–302.
[31] N. B. Morley, J. Burris, L. C. Cadwallader and M. D. Nornberg, “GaInSn usage in the research laboratory,” *Rev. Sci. Instrum.*, vol. 79, no. 5, p. 56107, 2008.
[32] V. Kocourek, C. Karcher, M. Conrath and D. Schulze, “Stability of liquid metal drops affected by a high-frequency magnetic field,” *Phys. Rev. E*, vol. 74, no. 2, Aug. 2006.
[33] U. Müller and L. Bühler, *Magnetofluiddynamics in channels and containers*. Springer Science & Business Media, 2001.
[34] D. Borin, “On the Magnetic Field Influence on the Viscosity of Liquid GaInSn with Suspended Solid Particles.”
[35] E. Monajjemi Rarani, N. Etesami and M. Nasr Esfahany, “Influence of the uniform electric field on viscosity of magnetic nanofluid (Fe3O4-EG),” *J. Appl. Phys.*, vol. 112, no. 9, p. 94903, 2012.
[36] C. Kasai, K. Namekawa, A. Koyano and R. Omoto, “Real-time two-dimensional blood flow imaging using an autocorrelation technique,” *IEEE Trans Sonics Ultrason*, vol. 32, no. 3, pp. 458–464, 1985.
[37] E.-M. Müller-Stüler, “Mathematische Analyse des Dopplersignals zur quantitativen Bestimmung des Blutflusses,” Philipps-Universität Marburg, Marburg, 2011.
[38] H. Murakawa, H. Kikura, and M. Aritomi, “Application of ultrasonic doppler method for bubbly flow measurement using two ultrasonic frequencies,” *Exp. Therm. Fluid Sci.*, vol. 29, no. 7, pp. 843–850, Aug. 2005.
[39] Y. Murai, Y. Tasaka, Y. Nambu, Y. Takeda, and S. R. Gonzalez A., “Ultrasonic detection of moving interfaces in gas–liquid two-phase flow,” *Flow Meas. Instrum.*, vol. 21, no. 3, pp. 356–366, Sep. 2010.
[40] M. Wu and M. Gharib, “Experimental studies on the shape and path of small air bubbles rising in clean water,” *Phys. Fluids*, vol. 14, no. 7, p. L49, 2002.
[41] A. Tomiyama, G. P. Celata, S. Hosokawa and S. Yoshida, “Terminal velocity of single bubbles in surface tension force dominant regime,” *Int. J. Multiph. Flow*, vol. 28, no. 9, pp. 1497–1519, 2002.
[42] J. de Vries, S. Luther and D. Lohse, “Induced bubble shape oscillations and their impact on the rise velocity,” *Eur. Phys. J. B*, vol. 29, no. 3, pp. 503–509, Oct. 2002.
[43] H. D. Mendelson, “The prediction of bubble terminal velocities from wave theory,” *AIChE J.*, vol. 13, no. 2, pp. 250–253, 1967.
[44] H. Lamb, Cambridge; New York: Cambridge University Press, 1932.
[45] W. L. Haberman and R. K. Morton, “An experimental investigation of the drag and shape of air bubbles rising in various liquids,” Navy Department “The David W. Taylor Model Basin,” Washington D.C., Technical Report DTMB-802, 1953.
[46] C. C. Maneri and H. D. Mendelson, “The rise velocity of bubbles in tubes and rectangular channels as predicted by wave theory,” vol. 14, no. 2, pp. 295–300, 1968.
[47] L.-S. Fan and K. Tsuchiya, *Bubble wake dynamics in liquids and liquid—solid suspensions*. Boston: Butterworth—Heinemann, 1990.
[48] S. Baz-Rodríguez, A. Aguilar-Corona and A. Soria, “Rising velocity for single bubbles in pure liquids,” *Rev. Mex. Ing. Quím.*, vol. 11, no. 2, pp. 269–278, 2012.
[49] I. H. Lehrer, “A rational terminal velocity euqationfor bubbles and drops at intermediate and high Reynolds numbers,” *J. Chem. Eng. Jpn.*, vol. 3, no. 9, pp. 237–240, 1976.
[50] M. Jamialahmadi, C. Branch and H. Müller-Steinhagen, “Terminal bubble rise velocity in liquids,” *Trans. Inst. Chem. Eng.*, vol. 72, no. 1, pp. 119–122, 1994.
[51] M. Krzan and K. Malysa, “Profiles of local velocities of bubbles in n-butanol, n-hexanol and n-nonanol solutions,” *Colloids Surf. Physicochem. Eng. Asp.*, no. 207, pp. 279–291, 2002.
[52] R. Clift, J. R. Grace and M. E. Weber, *Bubbles, Drops and Particles*. New York: Academic Press, Inc., 1978.
[53] S. Uno and R. C. Kintner, “Effect of Wall Proximity on the Rate of Rise of Single Air Bubbles in a Quiescent Liquid,” *AIChE*, vol. 2, no. 3, pp. 420–425, 1956.
[54] E. Loth, “Quasi-steady shape and drag of deformable bubbles and drops,” *Int. J. Multiph. Flow*, vol. 34, no. 6, pp. 523–546, Jun. 2008.

Appendix

Table 5. Data (B, U, d_{eq}) read from charts provided by Mori et.al. [1] (see Fig. 10 in their paper, Fig. 6 in this paper) and dimensionless parameters Eo, Re, N, N/C_D and C_D. The author estimates the read-off-error to be less than 1%. Physical properties of mercury according to C. Zhang et al. [55] with ρ = 13610 kg m^{-3}, η = 1.53 x 10^{-3} kg m^{-1} s^{-1}, σ = 0.460 N m^{-1}, σ_{el} = 1.0 x 10^{6} S m^{-1}.

B [T]	U [m s^{-1}]	d_{eq} [mm]	Eo [-]	Re [-]	N [-]	N/C_D [-]	C_D [-]
0	0.2447	1.74	0.8775	2631.90	0	0	0.3799
0.5	0.2475	1.74	0.8775	2662.06	0.1291	0.3408	0.3713
1.0	0.2299	1.74	0.8775	2473.06	0.5557	1.2917	0.4302
1.5	N/A	N/A	N/A	N/A	N/A	N/A	N/A
0	0.188	2.36	1.6200	2772.89	0	0	0.8585
0.5	0.203	2.36	1.6200	2914.95	0.2176	0.2801	0.7769
1.0	0.209	2.36	1.6200	2964.13	0.8560	1.1393	0.7513
1.5	0.178	2.36	1.6200	2603.51	2.1927	2.2516	0.9738
0	0.195	3.90	4.4113	4638.84	0	0	1.3784
0.5	0.190	3.91	4.4466	4476.35	0.3889	0.2596	1.4981
1.0	0.175	3.91	4.4466	4182.15	1.6652	0,9703	1.7163
1.5	0.162	3.94	4.4993	3806.47	4.1659	1.9752	2.1091
0	0.207	5.86	9.9518	7387.36	0	0	1.8417
0.5	0.165	5.88	10.0315	5826.08	0.6742	0.2250	2.9966
1.0	0.140	5.80	9.7672	5084.71	3.0084	0.7959	3.7797
1.5	0.127	5.82	9.8461	4424.97	7.8411	1.5522	5.0514

Table 6. Velocity U' (Mori, see Fig.9 in their paper, Fig. 7 in this paper)

B [T]	U' [m s^{-1}]	d_{eq} [mm]	Eo [-]	Re [-]	N [-]	N/C_D [-]	C_D [-]
0	0.2727	2.36	1.6164	3981.26	0	0	0.4151
0	0.2792	2.36	1.6164	4076.72	0	0	0.3959
0.3643	0.2538	2.36	1.6164	3706.11	0.0907	0.1893	0.4790
0.3584	0.2785	2.36	1.6164	4065.49	0.0800	0.2010	0.3981
0.5980	0.2612	2.36	1.6164	3812.80	0.2375	0.5247	0.4526
0.5980	0.2715	2.36	1.6164	3964.41	0.2284	0.5455	0.4186
0.6000	0.2812	2.36	1.6164	4104.80	0.2220	0.5686	0.3905
1.2396	0.2373	2.36	1.6164	3464.65	1.1228	2.0485	0.5481
1.2436	0.2565	2.36	1.6164	3745.41	1.0453	2.2287	0.4690
1.4020	0.2212	2.36	1.6164	3228.81	1.5411	2.4420	0.6311

Table 7: Rise velocity U at B = 0 T (Mori, see Fig.7 in their paper and Fig. 7 in this paper)

d_{eq} [mm]	U [m s^{-1}]
1.1966	0.2637
1.5243	0.2392
1.6810	0.2420
1.8377	0.2225
2.1939	0.1987
2.4218	0.1905
2.7780	0.1873
2.8777	0.1997
3.3336	0.1777
3.6898	0.1834
3.7895	0.1909
3.9035	0.1909
4.8580	0.1944
5.1571	0.1948
5.4421	0.1884
5.7270	0.2033
5.9264	0.1951

Table 8. Data of C. Zhang et al. [3] (see Fig. 3, p. 831 in their paper, Fig. 2 in this paper) , the present study, Schwarz & Fröhlich [19] (see Tab. 3, p. 141, Tab. 5, p. 149 and chap. 3.1.5, p. 140 in their paper, Fig. 3 in this paper) and J. Zhang et al. [20] (see Tab. III, p. 7 and Fig. 6, p .10 in their paper, Fig. 3 in this paper). As remarks the original data from the corresponding papers is given. (f.g. - fine grid, c.g. - coarse grid, s.h. - spherical harmonics)

C. Zhang			Present study		
d_{eq} [mm]	Eo [-]	u [mm s^{-1}]	d_{eq} [mm]	Eo [-]	u [mm s^{-1}]
4.2986	2.2	212.5	3.4777	1.42	198.667
4.6107	2.5	213.9	4.1551	2.03	207.604
5.4116	3.4	211.0	4.6171	2.50	217.826
6.0215	4.2	208.8	5.0744	3.01	229.153
6.4371	4.9	214.7	5.2805	3.14	216.996
7.0206	5.8	213.9	5.3342	3.33	220.969
7.5302	6.6	210.2	6.2802	4.62	226.676
8.3231	8.1	218.5			

Table 8 (cont.)

Schwarz			J. Zhang		
d_{eq} [mm]	u [mm s^{-1}]	remarks	d_{eq} [mm]	u [mm s^{-1}]	remarks
3.000	210.051	f.g. (*Eo* = 1.05, *Re* = 1822)	2.5145	253.496	(*Eo* = 0.74, *Re* = 1843)
4.600	226.670	c.g. (*Eo* = 2.5, *Re* = 3029)	3.2153	248.801	(*Eo* = 1.21, *Re* = 2313)
4.600	214.847	f.g. (*Eo* = 2.5, *Re* = 2871)	4.3355	223.126	(*Eo* = 2.20, *Re* = 2797)
4.600	227.269	s.h. (*Eo* = 2.5, *Re* = 3037)	6.4703	202.694	(*Eo* = 4.90, *Re* = 3792)

Table 9. Data of C. Zhang with magnetic field applied. Magnetic flux density B and velocity u are recalculated from N and C_D/C_D (B = 0 T) with u (B = 0 T) from Table 8 (see Fig. 3.18, p. 58 - VMF and Fig. 3.24, p. 63 - HMF in his PhD thesis [3], Fig. 8 & 9 in this paper).

Eo = 2.7, HMF		*Eo* = 4.4, HMF		*Eo* = 2.5, VMF		*Eo* = 4.9, VMF	
B [mT]	u [mm s^{-1}]	B [mT]	u [mm s^{-1}]	B [mT]	u [mm s^{-1}]	B [mT]	u [mm s^{-1}]
0	212.463	0	211.739	0	213.945	0	214.693
92.9	212.463	82.1	211.739	30.0	213.808	25.5	214.556
144.8	209.048	106.6	211.676	60.2	214.565	80.6	218.219
181.6	207.343	144.9	209.471	110.1	215.191	110.2	223.927
248.5	211.594	182.3	209.713	170.2	214.773	149.7	225.905
286.6	215.072	211.2	214.404	220.1	213.195	189.9	229.265
		248.5	219.563	290.3	211.056		
		287.7	224.963	299.7	204.227		

Table 10. Data of present study. *Eo* are given for B = 0 T (n – amount of bubbles, SD - standard deviation, Fig. 4 in this paper).

***Eo* (B = 0 T) = 1.42, D_a = 0.64 mm, $\dot{m}$ = 12.67 mm^{3}s^{-1}**					***Eo* (B = 0 T) = 3.01, D_a = 1.09 mm, $\dot{m}$ = 36.17 mm^{3}s^{-1}**						
B [mT]	d_{eq} [mm]	u [mm s^{-1}]	n [-]	SD d_{eq} [mm]	SD u [mm s^{-1}]	B [mT]	d_{eq} [mm]	u [mm s^{-1}]	n [-]	SD d_{eq} [mm]	SD u [mm s^{-1}]
0	3.4777	198.667	180	0.4330	7.1373	0	5.0744	227.211	193	0.2739	3.981
20.2	3.4033	198.528	181	0.4868	5.3803	20.2	5.0850	226.727	190	0.3179	3.370
36.5	3.3411	203.263	214	0.3558	4.5963	36.5	5.0798	226.396	192	0.3112	4.260
53.2	3.2978	205.340	226	0.3429	5.2223	53.2	5.0782	226.407	194	0.2652	2.905
70.4	3.2658	205.690	223	0.3668	4.7913	70.4	5.0831	225.258	199	0.1634	3.768
87.6	3.2386	205.782	247	0.2866	4.5770	87.6	5.0823	225.078	199	0.1583	3.600
105.1	3.2214	204.696	246	0.3062	3.9923	105.1	5.0871	224.562	201	0.1522	3.575
122.8	3.2119	204.265	251	0.3056	3.2403	122.8	5.0923	225.754	200	0.2011	3.909
140.3	3.2046	202.907	266	0.2240	3.8313	140.3	5.0961	225.142	197	0.1831	4.047
157.9	3.2012	202.419	269	0.1875	3.6727	157.9	5.1032	223.244	196	0.1747	3.206
175.5	3.2034	201.284	278	0.0897	3.4687	175.5	5.1015	225.229	197	0.1540	3.059
193.1	3.1717	200.502	294	0.0596	2.0443	193.1	5.1103	223.437	194	0.2100	1.766
210.9	3.1894	199.953	287	0.0350	2.0317	210.9	5.1141	223.653	196	0.1403	1.615
228.4	3.1857	203.209	289	0.0108	3.4607	228.4	5.1169	225.898	196	0.1733	2.017
245.6	3.1813	207.661	290	0.0100	4.1737	245.6	5.1282	228.403	192	0.2208	1.618
262.9	3.1837	209.829	290	0.0107	2.7693	262.9	5.1325	230.835	194	0.1560	1.110
280.6	3.1782	209.719	291	0.0081	1.0433	280.6	5.1390	231.334	188	0.2212	1.028
297.6	3.1786	210.137	291	0.0091	1.0963	297.6	5.1496	231.635	185	0.2804	1.355
315.9	3.1676	209.969	292	0.0088	1.1253	315.9	5.1489	231.377	189	0.2280	1.023
332.6	3.1763	210.595	292	0.0083	1.1830	332.6	5.1606	230.804	185	0.2764	1.019
349.7	3.1678	210.458	294	0.0094	0.8583	349.7	5.1826	228.944	178	0.3676	1.176
383.7	3.1731	207.528	293	0.0088	0.7873	383.7	5.1910	225.643	173	0.3718	1.322
416.9	3.1775	202.959	291	0.0090	0.5273	416.9	5.2092	220.259	174	0.3706	2.179
450.1	3.1749	197.327	292	0.0090	0.6380	450.1	5.2276	214.968	173	0.3584	1.160
482.5	3.1836	190.251	289	0.0096	0.5120	482.5	5.2519	208.753	168	0.4372	2.355
513.6	3.1864	185.209	288	0.0080	0.5003	513.6	5.3087	204.397	162	0.4662	2.659
586.1	3.1912	170.361	288	0.0083	0.3967	586.1	5.3203	192.814	158	0.4480	3.522
648.1	3.1995	159.229	285	0.0094	0.4063	648.1	5.4533	185.559	151	0.5538	2.717
697.7	3.2011	150.733	285	0.0075	0.3830	697.7	5.4624	180.048	154	0.6002	0.869
739.6	3.2026	144.984	285	0.0101	0.3557	739.6	5.4465	176.221	152	0.6120	0.836
772.6	3.2023	140.469	285	0.0099	0.3800	772.6	5.5243	173.380	150	0.4873	0.768
798.1	3.2191	137.048	279	0.0086	0.2887	798.1	5.7000	171.447	148	0.4972	1.112
818.5	3.2186	134.566	280	0.0076	0.2967	818.5	5.6527	169.455	149	0.4110	1.124
837.8	3.2261	132.602	279	0.0078	0.3380	837.8	5.6094	167.658	150	0.3623	1.100
852.9	3.2402	131.229	274	0.0080	0.3537	852.9	5.5461	165.848	151	0.2984	1.072
867.9	3.2317	129.405	276	0.0078	0.2983	867.9	5.5833	164.777	150	0.2919	1.226
880.4	3.2323	128.014	276	0.0084	0.2887	880.4	5.5543	162.992	151	0.2516	1.095
894.7	3.2349	126.622	275	0.0090	0.2813	894.7	5.5557	161.745	153	0.1930	0.760
906.7	3.2387	125.364	274	0.0086	0.2820	906.7	5.5711	160.698	151	0.1769	0.911
918.9	3.2413	124.165	275	0.0120	0.3330	918.9	5.6031	159.764	150	0.2002	1.215

Table 10 (cont.)

Eo (*B* = 0 T) = 3.14, D_a = 0.82 mm, $\dot{m}$ = 12.67 mm^{3}s^{-1}						*Eo* (*B* = 0 T) = 2.03, D_a = 0.64 mm, $\dot{m}$ = 12.67 mm^{3}s^{-1}					
B **[mT]**	d_{eq} **[mm]**	***u*** **[mm s^{-1}]**	***n*** **[-]**	SD d_{eq} **[mm]**	SD ***u*** **[mm s^{-1}]**	***B*** **[mT]**	d_{eq} **[mm]**	***u*** **[mm s^{-1}]**	***N*** **[-]**	SD d_{eq} **[mm]**	SD ***u*** **[mm s^{-1}]**
0	5.1802	214.430	60	0.3022	3.218	0	4.1687	213.201	43	0.2439	2.657
20.2	5.1662	214.100	63	0.2533	2.681	20.2	4.1563	212.802	43	0.3407	3.238
36.5	5.2132	215.501	66	0.1921	2.706	36.5	4.1551	211.469	43	0.0376	3.477
53.2	5.1470	215.046	66	0.2611	3.050	53.2	4.1469	211,173	44	0.0529	2.367
70.4	5.0789	215.130	69	0.2275	2.549	70.4	4.1377	210.110	44	0.0619	3.042
87.6	5.0849	215.299	72	0.0788	2.117	87.6	4.1351	210.202	44	0.0499	2.662
105.1	5.0877	214.330	69	0.0916	1.407	105.1	4.1401	209.008	44	0.0517	2.672
122.8	5.0879	213.930	72	0.0895	2.404	122.8	4.1353	209.395	44	0.0447	2.565
140.3	5.0917	214.170	71	0.1438	1.810	140.3	4.1394	208.208	44	0.0497	2.183
157.9	5.0945	213.880	70	0.1673	2.235	157.9	4.1315	207.371	44	0.0501	2.682
175.5	5.0925	215.120	71	0.0494	1.902	175.5	4.1544	205.174	43	0.0474	2.457
193.1	5.1056	216.010	69	0.1134	2.337	193.1	4.1432	204.271	44	0.0491	3.902
210.9	5.1117	217.071	69	0.1203	2.523	210.9	4.1356	204.146	44	0.0529	3.952
228.4	5.1170	216.790	69	0.1464	1.496	228.4	4.1509	205.913	43	0.0469	2.433
245.6	5.1179	221.933	69	0.1147	2.133	245.6	4.1581	207.284	43	0.0703	1.521
262.9	5.2039	224.087	69	0.3797	1.251	262.9	4.1612	208.766	43	0.0440	1.731
280.6	5.1330	226.646	69	0.0493	1.117	280.6	4.1522	213.848	43	0.0557	1.614
297.6	5.0767	229.064	69	0.1148	1.296	297.6	4.1534	215.797	43	0.0385	1.480
315.9	5.1899	229.379	69	0.1884	0.868	315.9	4.1574	216.357	43	0.0459	1.484
332.6	5.1545	228.993	72	0.0335	1.165	332.6	4.1559	216.459	43	0.0687	1.370
349.7	5.1612	229.293	68	0.0709	0.611	349.7	4.1610	216.656	43	0.0329	1.182
383.7	5.1961	226.338	66	0.1056	0.820	383.7	4.1632	213.791	43	0.0561	0.955
416.9	5.2021	221.544	66	0.0921	0.954	416.9	4.1664	210.984	43	0.0566	0.927
450.1	5.2098	216.540	65	0.0709	0.482	450.1	4.1799	206.254	43	0.0387	0.967
482.5	5.2294	211.242	66	0.0175	0.652	482.5	4.1727	200.899	42	0.0357	0.708
513.6	5.2402	206.497	64	0.0317	0.556	513.6	4.1825	194.480	42	0.0378	0.984
586.1	5.2965	194.604	65	0.0624	0.629	586.1	4.1818	181.255	42	0.0281	0.882
648.1	5.3216	185.784	64	0.0169	0.543	648.1	4.2054	171.155	42	0.0335	0.857
697.7	5.3545	179.414	63	0.0274	0.509	697.7	4.2084	165.044	42	0.0491	0.612
739.6	5.3757	174.781	63	0.0198	0.503	739.6	4.2033	159.711	42	0.0341	0.396
772.6	5.3855	171.468	62	0.0465	0.370	772.6	4.2025	155.388	42	0.0545	0.405
798.1	5.4111	168.937	60	0.0229	0.544	798.1	4.1775	152.922	42	0.0371	0.410
818.5	5.4203	167.051	59	0.0623	0.482	818.5	4.1994	151.181	42	0.0492	0.383
837.8	5.4139	165.424	57	0.0254	0.528						
852.9	5.4152	163.966	58	0.0238	0.596						
867.9	5.4423	162.711	59	0.0318	0.764						
880.4	5.4843	161.533	57	0.0715	0.554						
894.7	5.4772	160.807	57	0.1010	0.832						
906.7	5.4805	159.772	56	0.0387	0.666						
918.9	5.4968	158.825	55	0.0723	0.523						

Table 10 (cont.)

Eo (*B* = 0 T) = 2.50, D_a = 0.82 mm, $\dot{m}$ = 12.67 mm^{3}s^{-1}						*Eo* (*B* = 0 T) = 3.33, D_a = 0.82 mm, $\dot{m}$ = 12.67 mm^{3}s^{-1}					
B **[mT]**	d_{eq} **[mm]**	***u*** **[mm s^{-1}]**	***n*** **[-]**	SD d_{eq} **[mm]**	SD ***u*** **[mm s^{-1}]**	***B*** **[mT]**	d_{eq} **[mm]**	***u*** **[mm s^{-1}]**	***N*** **[-]**	SD d_{eq} **[mm]**	SD ***u*** **[mm s^{-1}]**
0	4.6171	217.826	32	0.1213	3.698	0	5.3342	220.969	21	0.0702	2.511
20.2	4.6119	217.441	32	0.0808	3.460	20.2	5.3738	217.386	20	0.0097	2.985
36.5	4.6177	217.999	31	0.0806	3.271	36.5	5.3716	216.586	20	0.0232	3.156
53.2	4.6346	216.117	31	0.0809	3.476	53.2	5.3741	216.624	20	0.0071	3.304
70.4	4.6280	216.528	31	0.0817	2.659	70.4	5.3688	217.648	20	0.0118	2.998
87.6	4.6175	216.749	31	0.0814	2.919	87.6	5.3701	216.697	20	0.0216	2.769
105.1	4.6212	215.738	31	0.0906	2.208	105.1	5.3803	215.861	20	0.0215	2.889
122.8	4.6442	215.578	31	0.0923	2.286	122.8	5.3825	217.045	20	0.0108	2.936
140.3	4.6299	214.488	31	0.1387	2.818	140.3	5.3907	216.697	20	0.0175	2.506
157.9	4.6310	213.263	31	0.0774	1.959	157.9	5.3816	219.153	20	0.0131	2.128
175.5	4.6268	214.093	31	0.0682	2.452	175.5	5.3973	220.829	20	0.0096	2.241
193.1	4.6436	215.081	31	0.1291	1.949	193.1	5.3993	222.008	19	0.0095	1.507
210.9	4.6370	216.382	31	0.0917	1.703	210.9	5.3972	223.179	20	0.0094	1.348
228.4	4.6153	217.067	31	0.1240	1.654	228.4	5.4096	224.872	19	0.0111	2.280
245.6	4.6338	218.352	30	0.0891	1.833	245.6	5.4116	225.905	19	0.0115	2.068
262.9	4.6646	220.453	30	0.1019	1.134	262.9	5.4180	226.124	20	0.0100	1.223
280.6	4.6354	223.028	30	0.1773	1.509	280.6	5.4179	227.533	19	0.0155	1.044
297.6	4.6145	225.216	31	0.1819	1.433	297.6	5.4324	228.634	19	0.0118	0.933
315.9	4.6504	225.357	30	0.1555	2.539	315.9	5.4341	228.749	19	0.0126	1.078
332.6	4.6610	225.489	30	0.2405	1.856	332.6	5.4423	228.883	19	0.0135	1.023
349.7	4.6997	224.184	30	0.1533	0.949	349.7	5.4537	228.961	19	0.0167	1.395
383.7	4.6939	219.920	30	0.1563	1.300	383.7	5.4745	227.811	19	0.0134	0.546
416.9	4.6881	215.175	30	0.2604	1.618	416.9	5.4948	224.572	18	0.0083	0.690
450.1	4.6894	209.774	30	0.2601	1.847	450.1	5.5100	219.144	18	0.0118	0.370
482.5	4.6934	204.883	30	0.2477	1.777	482.5	5.5352	213.484	18	0.0115	0.708
513.6	4.7259	199.393	30	0.2737	0.886	513.6	5.5480	207.673	18	0.0124	0.762
586.1	4.7213	186.627	30	0.2693	1.411	586.1	5.5998	197.686	18	0.0163	0.499
648.1	4.7668	176.609	29	0.3893	0.788	648.1	5.6330	188.695	17	0.0144	0.331
697.7	4.7297	167.945	28	0.4413	1.110	697.7	5.6738	182.336	17	0.0098	0.588
739.6	4.8127	162.903	28	0.2595	0.814	739.6	5.6947	177.196	17	0.0175	0.370
772.6	4.7909	159.168	28	0.3577	0.738	772.6	5.7063	173.885	17	0.0129	0.428
798.1	4.7602	156.175	28	0.4085	1.017	798.1	5.7148	171.225	17	0.0080	0.376
818.5	4.7911	153.675	28	0.4519	0.723	818.5	5.7227	169.694	16	0.0200	0.238

Table 10 (cont.)

Eo (B = 0 T) = 4.62, D_a = 1.02 mm, $\dot{m}$ = 18.18 mm^{3}s^{-1}					
B [mT]	d_{eq} [mm]	u [mm s^{-1}]	n [-]	SD d_{eq} [mm]	SD u [mm s^{-1}]
0	6.2802	226.676	21	0.8448	4.633
36.5	5.9359	224.209	27	0.3170	6.247
70.4	5.9022	221.241	24	0.5606	4.564
105.1	6.0841	222.281	24	0.3906	4.952
140.3	5.9684	226.523	24	0.4076	5.403
175.5	6.4126	234.573	22	0.4795	4.841
210.9	6.0586	235.508	24	0.4028	4.022
245.6	6.0682	238.225	22	0.5513	2.996
280.6	6.0322	239.374	22	0.5099	2.446
315.9	6.1486	240.236	23	0.4932	1.410
349.7	6.4117	240.232	22	0.5689	1.492
383.7	6.2865	235.637	22	0.5116	1.483
416.9	6.4733	231.839	21	0.3243	0.699
450.1	6.3367	228.617	22	0.2986	1.109
482.5	6.3784	223.569	22	0.3005	1.711
513.6	6.3823	219.923	21	0.3119	1.564
586.1	6.4573	209.273	21	0.3608	1.635
648.1	6.5858	198.346	20	0.4569	1.899
697.7	6.5934	193.554	19	0.3624	2.657
739.6	6.7678	186.305	20	0.4003	3.314
772.6	6.5657	183.477	19	0.35350	3.923
798.1	6.7050	182.977	19	0.3050	3.104
818.5	6.5564	181.725	19	0.2684	3.188